

Observation-based quantification of physical processes that impact sea level

Sjoerd Groeskamp¹

¹Royal NIOZ Netherlands Institute for Sea Research, 't Horntje (Texel), Netherlands

Correspondence: Sjoerd Groeskamp (sjoerd.groeskamp@nioz.nl)

Abstract. This study provides observationally based estimates of the contributions to sea level rise from individual physical oceanographic processes. The kinematic equation for sea level evolution is used to calculate the spatial distribution of the evolution of sea level rise, and its global integral. Results are separated into impacts from boundary mass fluxes and from non-Boussinesq steric effects. The non-Boussinesq steric effect itself is further decomposed into contributions from boundary buoyancy fluxes and interior buoyancy changes driven by mixing processes. It is neither the intention nor currently possible to close the global mean sea level (GMSL) budget using this approach. Instead, the results quantify the magnitude and uncertainty of the physical oceanographic processes and their relative importance in shaping GMSL rise. This allows for a comparison of the impact on GMSL by single processes or parameterizations. Results indicate large uncertainties associated with boundary heat, mass, and freshwater fluxes and highlight the importance of ocean mixing for GMSL rise. Additionally, GMSL rise is substantially affected by how shortwave radiation is redistributed with depth and by the choice of neutral physics calculation method. This study also finds that nonlinear thermal expansion is offset by mixing-induced densification, and that both processes strongly influence sea level as consequences of the nonlinear equation of state. Many of the results are relevant for observationally based calculations and for modelers making decisions about which methods or parameterizations to use. Understanding the impact of these processes on GMSL rise, and how they change in a transient ocean and climate system, is important because these choices influence projections of future sea level rise, which inform policy decisions.

1 Introduction

Since 1850, human-induced warming has increased global surface temperatures by approximately 1.1 °C (Eyring et al., 2023). About 89% of this anthropogenic heat has been absorbed by the ocean (von Schuckmann et al., 2020), leading to significant ocean warming (Li et al., 2023), thermal expansion and associated sea level rise (Horwath et al., 2022). Approximately 4% of the warming since the pre-industrial era has contributed to the melting of glaciers and ice sheets, further elevating global sea level. The remaining heat has been stored in land (6%) and the atmosphere (1%).

Global mean sea level (GMSL) rise is estimated using satellite altimetry (Ablain et al., 2017; Hamlington et al., 2024) and tide gauges (Jevrejeva et al., 2006; Hamlington et al., 2022). Since 1901, GMSL has risen by approximately 21 cm (Fox-Kemper et al., 2023). Sea level rise has accelerated from 1.35 mm year⁻¹ between 1901 and 1990 to 3.7 mm year⁻¹ between 2006 and 2018 (chapter 9, table 9.5, Fox-Kemper et al. (2023), Nerem et al. (2018)), and it is projected to accelerate further

(Nerem et al., 2022). Currently, the main contributions to sea level rise are thermal expansion (39%, 1.4 mm year⁻¹) and the combined contributions from glaciers and ice sheets (45%, 1.6 mm year⁻¹).

The GMSL rise budget can be closed by summing contributions from steric and barystatic changes. Steric sea level change is obtained by integrating global ocean temperature and salinity observations (Pattullo et al., 1955; Antonov et al., 2002) and accounted for roughly 34% of GMSL rise between 1900 and 2018 (Frederikse et al., 2020). Barystatic change, derived from satellite observations of mass fluxes from glaciers, ice sheets, and terrestrial water storage (Shepherd et al., 2018; Fasullo and Nerem, 2018), contributed approximately 66% of GMSL rise over the same period (Frederikse et al., 2020). These "top-down" approaches have enabled the closure of GMSL budgets within statistical uncertainty (Moore et al., 2011; Horwath et al., 2022; Frederikse et al., 2020; Church et al., 2011; Ludwigsen et al., 2024).

Instead of a top-down approach, this study uses a 'bottom-up' strategy, estimating GMSL as the sum of contributions from individual physical oceanographic processes that alter ocean density and volume. The kinematic equation for sea level evolution is used to calculate the impacts of boundary mass fluxes and non-Boussinesq steric effects on sea level rise. Non-Boussinesq steric effects are further decomposed into contributions from boundary freshwater, heat, and salt fluxes, and from interior diffusive and advective fluxes generated by oceanic turbulent eddies. This bottom-up approach was previously applied by Griffies and Greatbatch (2012) within numerical models, successfully closing the model's GMSL budget.

This study uses observation-based datasets instead of numerical models to quantify sea level changes caused by physical oceanographic processes. This allows for an assessment of how uncertainties in observations or parameterizations influence GMSL calculations and how these compare to observed GMSL rise rates. Rates of sea level rise are calculated using annual-mean observational hydrography, representing annual-mean changes. Results are presented as spatially varying maps of local sea level changes and as their global integrals to estimate GMSL rise. However, due to large uncertainties in observational products, it is neither intended nor possible at this stage to observationally close the GMSL budget using this approach. This highlights the lack of observational constraints on air-sea interactions, mass fluxes, and mixing, as well as incomplete understanding and representation of fundamental physical mechanisms underlying GMSL budgets.

Specifically, this study examines the impacts of variations in heat, mass and freshwater flux products, mixing strength parameterizations, neutral physics, shortwave radiation depth penetration parameterizations, and eddy stirring parameterizations. All of these processes substantially influence GMSL rise, with first-order impacts of the order of millimeters per year. These results are relevant for numerical ocean and climate models, as modelers must make decisions on how to represent these processes, which in turn affect projections of future sea level rise. Quantifying the impact of different parameterizations on GMSL in numerical ocean models is difficult due to the complexity and expense of reprogramming and rerunning the model and because of difficulties to isolate the impact of a single change.

1.1 Nonlinear thermal expansion and densification upon mixing

This study also investigates whether "densification upon mixing" can prevent the ocean from ever expanding due to warming (Schanze and Schmitt, 2013). Even without anthropogenic warming, an ocean with a net-zero global heat flux would still

expand, causing sea level rise. This occurs because the thermal expansion coefficient α varies with temperature (and to a lesser extent, salinity and pressure). Warmer water expands more than colder water contracts.

Since ocean warming primarily occurs in low latitudes over warm waters and cooling occurs at higher latitudes over colder waters, warming drives greater expansion than cooling drives contraction. Globally integrated, this produces a net ocean volume increase that contributes to GMSL (Griffies and Greatbatch, 2012; Schanze and Schmitt, 2013). This study refers to this process as "nonlinear thermal expansion" as it occurs only due to nonlinearity of the equation of state, distinct from the thermal expansion caused by a net heat flux into the ocean. It should not be confused with the thermobaric effect or thermobaricity, which arises from variations in the thermal expansion coefficient with pressure.

Densification upon mixing can reduce sea level (Gille, 2004; Jayne et al., 2004) and thereby counteract nonlinear thermal expansion. This occurs when two water parcels mix, and the resulting mean density is greater than the average of the original densities due to the nonlinear equation of state. This process, also known as cabbeling (Witte, 1902; Foster, 1972; McDougall, 1987b), contracts water volume and lowers sea level. As first suggested by McDougall and Garrett (1992), densification upon mixing opposes nonlinear thermal expansion, potentially preventing unbounded ocean expansion. While Schanze and Schmitt (2013) estimated the magnitude of densification upon mixing using air-sea heat fluxes, it has not been verified from independent sources, that this is of the same order as nonlinear thermal expansion. This study addresses that gap.

This paper is organized as follows. Section 2 derives the equations governing physical oceanographic processes influencing the GMSL budget and discusses assumptions and processes not covered. Section 3 describes the datasets used. Section 4 presents results for nonlinear thermal expansion (section 4.3), densification upon mixing (section 4.6), shortwave radiation (section 4.4), and stirring (section 4.7), among others. Section 5 provides a summary, discussion of caveats, and implications, followed by a brief conclusion in Section 6.

2 Theory

Sea level changes due to adding or redistributing mass, and due to changes in ocean density (Gill and Niller, 1973). Following Griffies and Greatbatch (2012) (their Eq. 1), these effects are described using the kinematic equation for sea level evolution:

$$\underbrace{\frac{\partial \eta}{\partial t}}_{\text{sea level evolution}} = \underbrace{\frac{Q_{\text{mass}}}{\rho(z=\eta)}}_{\text{boundary mass flux}} - \underbrace{\nabla \cdot \int_{-H}^{\eta} \mathbf{u} dz}_{\text{dynamic changes}} - \underbrace{\int_{-H}^{\eta} \frac{1}{\rho} \frac{d\rho}{dt}}_{\text{Non-Boussinesq steric}}. \quad (1)$$

Here both integrals are from the ocean bottom height ($-H$) to the ocean surface height (η). Sea level evolution (l.h.s. of Eq. 1) is evaluated locally for a vertical water column by taking the sum of i) the boundary mass fluxes, ii) the redistribution of ocean volume by ocean currents (dynamic changes), and iii) Non-Boussinesq steric changes. The latter is the expansion or contraction of seawater volume due to changes in sea water density. Changes in sea water density are due to small-scale or mesoscale mixing processes, due to air-sea heat, mass and freshwater fluxes, or due to geothermal heating (see Appendix A for details). Eq. 1 is derived under the assumptions that the ocean bottom does not move, the ocean surface area is constant and

that the gravitational acceleration is constant (Griffies and Greatbatch, 2012). Processes not covered are the inverse barometer effect, the tidal sea surface elevations and joule heating (Griffies and Greatbatch, 2012).

This study presents both maps of the spatial structure of sea level evolution, as well as the global integral of these maps that provide the net GMSL changes. The spatial structure is given by applying Eq. 1 to a vertical water column, while its impact on GMSL rise $\frac{\partial \bar{\eta}}{\partial t}$ is obtained by integrating those results globally, using:

$$\frac{\partial \bar{\eta}}{\partial t} = \frac{1}{\mathcal{A}} \int_{\text{globe}} \frac{\partial \eta}{\partial t} dA, \quad \text{with} \quad \mathcal{A} = \int_{\text{globe}} dA. \quad (2)$$

Under a no-flux boundary condition, the term "dynamic changes" in Eq. 1 vanishes (second term, r.h.s.). Therefore, ocean currents have no net effect on GMSL rise and instead only redistribute volume.

In the remainder of this section the sea level calculations for the boundary mass fluxes (section 2.1) and redistribution of ocean volume by ocean currents (section 2.4), are specified. This study presents sea level calculations of the non-Boussinesq steric changes due to diffusive salt and heat fluxes (section 2.3), skew fluxes of salt and heat (section 2.4), and by the combination of direct and indirect boundary fluxes of salt and heat (section 2.2). The details of most derivations are moved to the appendices. Derivations rely heavily on (Griffies and Greatbatch, 2012) and (Groeskamp et al., 2019b).

2.1 Sea level change due to a boundary mass fluxes

At the ocean boundaries, the ocean mass flux Q_{mass} ($\text{kg s}^{-1} \text{ m}^{-2}$) is defined as positive into the ocean and given by:

$$Q_{\text{mass}} = P - E + R + I + A_e, \quad (3)$$

where P is precipitation (positive into the ocean), E is evaporation (positive out of the ocean), R is runoff from rivers (positive into the ocean), I is runoff from land ice melt (positive into the ocean), and A_e is the aeolian deposition of salt (positive into the ocean). These mass fluxes can enter the ocean by crossing the ocean surface (E , P , and A_e), laterally (R) or from both directions (I). Inserting Eq. 3 into the first term on the r.h.s. of Eq. 1 leaves:

$$\left. \frac{\partial \eta}{\partial t} \right|_{\text{mass}} = \frac{Q_{\text{mass}}}{\rho(\eta)} = \frac{1}{\rho(\eta)} (P - E + R + I + A_e). \quad (4)$$

When Eq. 4 is integrated globally, even for a net-zero global mean mass flux, there can still be a net contribution to GMSL rise. This is because the impact of the mass flux on volume is weighted by the sea surface density $\rho(\eta)$ (section 4.1). This effect is conceptually similar to the impact of a changing thermal expansion coefficient for a net-zero global heat-flux as previously mentioned in section 1 and detailed in Appendix B.

2.2 Sea level change due to boundary heat, salt and freshwater fluxes

Boundary mass fluxes into the ocean (e.g., evaporation, precipitation, ice melt), as well as direct sources of heat and salt, all impact sea level. The impact of such boundary fluxes on sea level rise can be expressed as:

$$\left. \frac{\partial \eta}{\partial t} \right|_{\text{boundary}} = - \int_{-H}^{\eta} \frac{1}{\rho} (F_{\text{mass}}^{\rho} + F_{\text{surface}}^{\rho} + F_{\text{geo}}^{\rho} + F_{\text{swr}}^{\rho}) dz \quad (5)$$

115 The details for deriving Eq. (5) can be found in Appendix B. The term F_{mass}^ρ ($\text{kg m}^{-3} \text{s}^{-1}$) represents the changes in local
ocean density due to ocean mass fluxes (Q_{mass}), primarily through alterations of local salinity. Here F_{surface}^ρ ($\text{kg m}^{-3} \text{s}^{-1}$)
captures the impact on density by direct sources of salinity and heat at the surface of the ocean. Surface salt fluxes (e.g., due
to sea ice melt or sea spray) are not considered in this analysis, because they are unknown or negligible. Surface heat fluxes
are longwave radiation as well as latent and sensible heat fluxes. Shortwave radiation (SWR) enters the ocean surface and
120 can penetrate to deeper layers depending on the clarity of the water (Paulson and Simpson, 1977). The impact of shortwave
radiation on ocean density is represented by the term F_{swr}^ρ ($\text{kg m}^{-3} \text{s}^{-1}$) and is a term separate from F_{surface}^ρ . Geothermal
heating at the sea floor is given by F_{geo}^ρ and has a small impact on ocean density (de Lavergne et al., 2015).

2.3 Sea Level Change due to diffusive fluxes

In this section an expression is derived for the impact of diffusive mixing on density and sea level. Mixing is split into a
125 contribution from mesoscale and small-scale processes (Fox-Kemper et al., 2019). Small-scale mixing is due to eddies on the
order of a meter that are most commonly associated with breaking internal waves and boundary-layer processes (MacKinnon
et al., 2013; Large et al., 1994). This mixing is represented by a vertical turbulent diffusivity D acting on vertical tracer
gradients (McDougall et al., 2014). The magnitude of the vertical eddy diffusivity is typically of $\mathcal{O}(10^{-5} - 10^{-3} \text{ m}^2 \text{ s}^{-1})$
(Polzin et al., 1997; Whalen et al., 2012; de Lavergne et al., 2020). Mesoscale eddies of $\mathcal{O}(20\text{-}200 \text{ km})$ that stir tracers along
130 neutral directions are parameterized by isoneutral eddy diffusivity K_N acting on tracer gradient along a neutral direction $\nabla_N C$
(Redi, 1982; Griffies, 1998; McDougall et al., 2014). When influenced by the geometric constraints of the surface boundary,
mesoscale stirring leads to horizontally oriented mixing across outcropped density surfaces (Tandon and Garrett, 1997; Treguier
et al., 1997; Ferrari et al., 2008), which is parameterized by a horizontal diffusivity K_H acting on horizontal tracer gradient
 $\nabla_H C$. The magnitude for K_N and K_H is typically $\mathcal{O}(10^1 - 10^3 \text{ m}^2 \text{ s}^{-1})$ (Abernathey and Marshall, 2013; Klocker and
135 Abernathey, 2013; Cole et al., 2015; Roach et al., 2018; Groeskamp et al., 2017, 2020; Sévellec et al., 2022; Kusters et al.,
2024).

The above mixing directions are represented by a symmetric positive-definite kinematic diffusivity tensor \mathbf{K} ($\text{m}^2 \text{s}^{-1}$) that
contains the contributions of the mesoscale neutral and horizontal diffusion, and small-scale isotropic diffusion. This leads
to the following expression for the impact of diffusive mixing on density and sea level, for which the details are provided in

$$\begin{aligned}
\left. \frac{\partial \eta}{\partial t} \right|_{\text{diffusion}} &\approx \underbrace{-\nabla_{\text{H}} \cdot \int_{-H}^{\eta} \mathbf{R}^{\text{hor}} dz}_{\text{Redistribution}} + \underbrace{\mathbf{R}^{\text{hor}}(\eta) \cdot \nabla_{\text{H}} \eta - \mathbf{R}^{\text{hor}}(-H) \cdot \nabla_{\text{H}}(-H)}_{\text{diffusion-boundary interaction}} \\
&+ \underbrace{\int_{-H}^{\eta} K_{\text{H}}^{-1} |\mathbf{R}^{\text{hor}}|^2 dz + \int_{-H}^{\eta} D^{-1} |\mathbf{R}^{\text{ver}}|^2 dz - \int_{-H}^{\eta} \rho g \kappa \mathbf{k} \cdot \mathbf{R}^{\text{ver}} dz}_{\text{diffusion-density interaction}} \\
&+ \underbrace{\int_{-H}^{\eta} P_{\text{T}_b}^{\text{tr}} + P_{\text{C}_b}^{\text{tr}} + P_{\text{C}_b}^{\text{hor}} + P_{\text{T}_b}^{\text{ver}} + P_{\text{C}_b}^{\text{ver}} dz}_{\text{Cabbeling and Thermobaricity}}, \tag{6}
\end{aligned}$$

where the following definitions (see Appendix C) apply:

$$\mathbf{R} = -\alpha \mathbf{K} \cdot \nabla \Theta + \beta \mathbf{K} \cdot \nabla S_A, \tag{7}$$

$$P = \nabla \alpha \cdot (\mathbf{K} \cdot \nabla \Theta) - \nabla \beta \cdot (\mathbf{K} \cdot \nabla S_A). \tag{8}$$

145 Here Θ is Conservative Temperature (McDougall, 2003; Graham and McDougall, 2013), S_A is Absolute Salinity (McDougall et al., 2012; Millero et al., 2008). Further, \mathbf{R}^{tr} , \mathbf{R}^{hor} , and \mathbf{R}^{ver} (m s^{-1}) are the components of \mathbf{R} for the three different mixing direction "neutral", "horizontal" and "vertical", respectively. Then P^{tr} , P^{hor} , and P^{ver} are the components of P (s^{-1}) for the three different mixing direction. For the neutral direction $\alpha \nabla_{\text{N}} \Theta = \beta \nabla_{\text{N}} S_A$, and thus $\mathbf{R}^{\text{tr}} = 0$. The first term on the r.h.s. of Eq. 6 named "redistribution" turns out to be large, but also globally integrates to zero due to the divergence operator.

150 By explicitly writing Eq. 6 in a form that contains this redistribution term, this creates the term named "diffusion-density interaction" that can be interpreted as the interaction between diffusion and density gradients. This term will turn out to be small, such that it is advantageous to write Eq. 6 in this form, as it allows for neglecting the global integration of the redistribution term and the diffusion-density interaction term. The term named "Production" is the interaction between diffusion and the nonlinear equation of state. This term includes the terms causing densification upon mixing, cabbeling and the thermobaric terms, as
155 specified in Appendix C1. Thermobaricity can in fact lead to both an increase and decrease in density, but its impact on density is generally an order of magnitude smaller than that due to cabbeling (Klocker and McDougall, 2010; Groeskamp et al., 2016). Although cabbeling and thermobaricity are names specifically referring to neutral mixing (McDougall, 1987b), effects of the nonlinear equation of state that change density due to mixing of Θ and S_A , are not limited to the neutral direction. The same abbreviations for the mixing directions as before are used for the impact of cabbeling ($P_{\text{C}_b}^{\text{tr}}$, $P_{\text{C}_b}^{\text{hor}}$, $P_{\text{C}_b}^{\text{ver}}$) and thermobaricity
160 ($P_{\text{T}_b}^{\text{tr}}$, $P_{\text{T}_b}^{\text{hor}}$, $P_{\text{T}_b}^{\text{ver}}$), due to the different mixing processes.

2.4 Sea level change due to ocean dynamics and eddy-induced transport

The convergence of the vertically integrated horizontal ocean velocity \mathbf{u} can lead to redistribution of volume and thus a local impact on sea level, while its global integral is zero under the assumption that there is no velocity through the boundaries. The

velocity \mathbf{u} will be approximated as the sum of the geostrophic velocity \mathbf{u}_{geo} and the eddy-induced velocity \mathbf{u}_{eddy} , to obtain:

$$165 \quad \mathbf{u} = \mathbf{u}_{\text{geo}} + \mathbf{u}_{\text{eddy}}. \quad (9)$$

Following Ferrari et al. (2010), the eddy velocity parameterization is constructed to ensure a net zero vertical integral over the local eddy velocity in Eq. 1 (Appendix D), leaving:

$$\left. \frac{\partial \eta}{\partial t} \right|_{\text{dynamic}} = -\nabla \cdot \int_{-H}^z \mathbf{u}_{\text{geo}} dz. \quad (10)$$

Hence, there is no impact of dynamic changes on the GMSL budget, but locally the dynamics do change sea level. The latter
170 can be estimated using the thermal wind balance in combination with a reference level velocity.

Although the eddy-induced transport itself does not change sea level, it does impact density through unrepresented transport of salt and heat (Griffies and Greatbatch, 2012). The resulting impact of stirring on sea level evolution is given by:

$$\left. \frac{\partial \eta}{\partial t} \right|_{\text{stirring}} = \underbrace{-\nabla_H \cdot \int_{-H}^{\eta} \mathbf{R}_{\text{stir}} dz}_{\text{Redistribution}} + \underbrace{\int_{-H}^{\eta} P_{\text{stir}} dz}_{\text{Production}} + \underbrace{\int_{-H}^{\eta} \mathbf{R}_{\text{stir}} \cdot \nabla \ln \rho dz}_{\text{Eddy-density interaction}}. \quad (11)$$

The full derivation for obtaining Eq. 11 is given in Appendix D. Note that the down gradient eddy tracer flux of temperature
175 and salinity are embedded inside \mathbf{R}_{stir} (m s^{-1}) and P_{stir} (s^{-1}) in a manner comparable to that for diffusion:

$$\mathbf{R}_{\text{stir}} = -\alpha \mathbf{K}_{\text{stir}} \cdot \nabla \Theta + \beta \mathbf{K}_{\text{stir}} \cdot \nabla S_A, \quad (12)$$

$$P_{\text{stir}} = -\nabla \alpha \cdot (\mathbf{K}_{\text{stir}} \cdot \nabla \Theta) + \nabla \beta \cdot (\mathbf{K}_{\text{stir}} \cdot \nabla S_A). \quad (13)$$

Here \mathbf{K}_{stir} is the stirring strength operator (Eq. D3), also known as the "GM diffusivity" (Gent and McWilliams, 1990). The first term on the r.h.s. of Eq. 11 named - redistribution - globally integrates to zero, while the last term, named "Eddy-density interaction" will be small. Hence, when integrating Eq. 11 globally, it is the Production term in Eq. 11 that will lead to the main impact of stirring on GMSL rise. This term is related to the interaction between stirring and the nonlinearity equation of state,
180 comparable to the cabbeling and thermobaricity terms for diffusion.

2.5 Sea level change due to the Non-Neutrality term

A term that does not exist in the real ocean, but does exist in any calculation involving neutral mixing, is the "non-neutrality" term related to neutral physics (Griffies, 2004; Klocker et al., 2009). Diffusive fluxes and stirring in the neutral direction are calculated using the slopes of the neutral tangent plane, and the tracer gradients along the neutral tangent plane (McDougall,
185 1987a; McDougall and Jackett, 1988). The accuracy with which one can calculate the neutral slopes or gradients, depends strongly on the method used (McDougall and Jackett, 1988; Stanley, 2019; Stanley et al., 2020; Groeskamp et al., 2019a). When a neutral slope or gradient is not exact, this will lead to fictitious diffusion (Klocker et al., 2009) that causes additional densification upon mixing (Groeskamp et al., 2019a), and therefore impacts steric sea level calculations. This means that; i)

$\mathbf{R}^{\text{ntr}} \neq 0$, ii) that the \mathbf{P}^{ntr} terms also have error embedded, and iii) that the neutral slopes in the stirring term are not exact. This
 190 allows us to define the non-neutrality term as:

$$\begin{aligned}
 \left. \frac{\partial \eta}{\partial t} \right|_{\text{non-neutral}} &\approx - \underbrace{\nabla_{\mathbf{H}} \cdot \int_{-H}^{\eta} \mathbf{R}^{\text{ntr}} dz}_{\text{Redistribution}} - \mathbf{R}^{\text{ntr}}(-H) \cdot \nabla_{\mathbf{H}}(-H) \\
 &+ \int_{-H}^{\eta} K_{\text{N}}^{-1} |\mathbf{R}^{\text{ntr}}|^2 dz + \int_{-H}^{\eta} \kappa \nabla_{\text{N}} P \cdot \mathbf{R}^{\text{ntr}} dz \\
 &+ \int_{-H}^{\eta} \mathbf{P}^{\text{ntr}} - \mathbf{P}^{\text{(perfectly neutral)}} dz + \left. \frac{\partial \eta}{\partial t} \right|_{\text{stirring}}^{\text{non-neutral}}. \tag{14}
 \end{aligned}$$

Here $\mathbf{R}^{\text{ntr}}(\eta) \cdot \nabla_{\mathbf{H}} \eta = 0$ as there are no neutral slopes at the surface, and $\mathbf{P}^{\text{(ntr)}} = \mathbf{P}^{\text{(perfectly neutral)}} + \mathbf{P}^{\text{(error)}}$. Hence, $\mathbf{P}^{\text{(error)}}$ is
 195 the impact of an incorrect neutral physics calculation scheme. If $\mathbf{P}^{\text{(error)}} > 0$ then the method underestimates neutral gradients, while for $\mathbf{P}^{\text{(error)}} < 0$, the method overestimates neutral gradients. In the latter case, which is most common, this can be interpreted as enhanced vertical mixing and leads to additional, but non-realistic densification upon mixing. Note that the vertical component of the $\mathbf{R}^{\text{ntr}} \cdot \mathbf{k}$ has no role to play at all, because there are no vertical gradients of either the bottom slope or the surface slope, and this term is zero after vertical integration. The last term $\left. \frac{\partial \eta}{\partial t} \right|_{\text{stirring}}^{\text{non-neutral}}$ is the impact of stirring along
 200 non-neutral slopes, as detailed in Appendix D. For this term, an overestimation of the neutral slopes will lead to more reduction in GMSL.

2.6 The total sea level rise equation

Collecting all terms, the local evolution of sea level rise can be expressed as:

$$\frac{\partial \eta}{\partial t} = \underbrace{\left. \frac{\partial \eta}{\partial t} \right|_{\text{mass}}}_{\text{Eq.4}} + \underbrace{\left. \frac{\partial \eta}{\partial t} \right|_{\text{boundary}}}_{\text{Eq.5}} + \underbrace{\left. \frac{\partial \eta}{\partial t} \right|_{\text{diffusion}}}_{\text{Eq.6}} + \underbrace{\left. \frac{\partial \eta}{\partial t} \right|_{\text{dynamic}}}_{\text{Eq.10}} + \underbrace{\left. \frac{\partial \eta}{\partial t} \right|_{\text{stirring}}}_{\text{Eq.11}} + \underbrace{\left. \frac{\partial \eta}{\partial t} \right|_{\text{non-neutral}}}_{\text{Eq.14}} \tag{15}$$

205 Each of these terms comprises many processes that also vary in space and time, emphasizing the number of fundamental processes that need to be understood in order to provide an accurate bottom-up calculation of the evolution of sea level and its global integral for calculating GMSL rise. Section 3 described the data used for calculating these terms. Section 4 shows the results.

3 Data used

210 This section describes a range of observational products that are needed for calculating the terms in the GMSL budget as defined in section 2. An overview is given in Table 1.

Variable	Source
$\Theta, S_A, P, N^2, C_b, T_b,$ $R_\rho, \alpha, \beta, \rho, z_{\text{mld}}, \nabla_H(-H)$	Using t, S_p and P from World Ocean Atlas 2018 (Garcia et al., 2019), and recalculated using McDougall and Barker (2011)
K_N, K_H and K_{stir}	Based on K from Groeskamp et al. (2020).
D	Based on D from de Lavergne et al. (2020)
Latent and sensible heat. Longwave and shortwave radiation. Evaporation, Precipitation, Runoff	From two products for comparison; 1) the "OA" Fluxes (Yu and Weller, 2007), and 2) the "CORE.v2" Fluxes (Yeager and Large, 2008)
$\nabla_N \Theta, \nabla_N P, \nabla_N S_A$	Using the VENM software of Groeskamp et al. (2019a)
Geothermal Heating	Based on de Lavergne et al. (2015); Goutorbe et al. (2011)

Table 1. Presented are the sources of the different variables considered in this study. The mixed layer depth z_{mld} is calculated using de Boyer Montégut et al. (2004). Direct salt sources and Aeolian fluxes are not considered. Land ice melt I is embedded in R for both OA and CORE.v2. Further details are described in section 3.

3.1 Gridded climatology

World Ocean Atlas 2018 (Garcia et al., 2019) is used for objectively analyzed (1° grid) climatological fields of *in situ* temperature t and practical salinity S_p at standard depth levels for monthly compositing periods for the world ocean sometimes referred
215 to as a "standard year". Monthly means for the upper 1500 m are used, while it is assumed that the deep ocean has little seasonal variation, such that seasonal means (repeated per quarter) are used for the interior (below 1500 m). Topographic gradients (e.g. $\nabla_H(-H)$ in Eq. 6) are calculated using vertical derivatives from WOA column depths. TEOS-10 software (IOC et al., 2010; McDougall and Barker, 2011) is applied to convert (S_p, t, P) into (S_A, Θ, P) . Subsequently TEOS-10 software is further used to take (S_A, Θ, P) as input and calculate the mixed layer depth z_{mld} according to the de Boyer Montégut et al. (2004) criteria,
220 the Buoyancy frequency N^2 , the expansion coefficients and their gradients, and the cabling and thermobaricity coefficients (C_b, T_b). Static stability or a stably stratified water column ($N^2 > 0$ everywhere) is obtained using a minimal adjustment of S_A and Θ within the measurement error (Jackett and McDougall, 1995; Barker and McDougall, 2020).

3.2 Diffusivities for diffusion and stirring

The mesoscale neutral K_N and horizontal K_H diffusivities are based on the product from Groeskamp et al. (2020). They
225 provide global 3D observational-based estimates of oceanic mesoscale diffusivity on a gridded climatology of WOA18 using a combination mixing length theory (Prandtl, 1925), mean flow suppression theory (Ferrari and Nikurashin, 2010; Klocker et al., 2012), and the theory of vertical modes (LaCasce and Groeskamp, 2020). As the diffusivities obtained by Groeskamp et al. (2020) are static, they are repeated for each month to obtain estimates for K_N, K_H and K_{stir} . To separate between neutral and horizontal mesoscale mixing, a step-wise change is applied at the base of the mixed layer. Above the mixed layer
230 depth, mixing is represented by horizontal mesoscale mixing and below the mixed layer depth, it is represented by neutral

mixing. The same mesoscale diffusivities are used to approximate the mesoscale stirring diffusivities K_{stir} , thus assuming that stirring diffusivities are equal to tracer diffusivities, even though they are known to vary spatially (Smith and Marshall, 2009; Abernathy et al., 2013; Kusters et al., 2025).

Vertical mixing diffusivities are based on de Lavergne et al. (2020), which is a parameterization for turbulence production due to internal tides (de Lavergne et al., 2019, 2020). This parameterization does not include surface boundary layer mixing processes, such as those parameterized with the K-profile parameterization (KPP) scheme (Large et al., 1994). Griffies and Greatbatch (2012) found that in a numerical model, the KPP scheme leads to 0.3 mm year^{-1} GMSL rise (see their Table 1), which we will be missing.

This study also make use of constant diffusivities of $D = 5 \times 10^{-5} \text{ m}^2 \text{ s}^{-1}$, $K_N = K_{\text{stir}} = 300 \text{ m}^2 \text{ s}^{-1}$, $K_H = 750 \text{ m}^2 \text{ s}^{-1}$, while maintaining the mixed-layer depth as the separation.

3.3 Neutral slopes and gradients

For the calculation of neutral slopes and gradients, two methods are applied. Traditionally neutral slopes and gradients are calculated using the "local" method that computes the ratio of the horizontal to vertical derivative of σ_t , i.e. the locally referenced potential density (Redi, 1982; Griffies, 1998). The resulting slopes are then combined with the local spatial gradients of S_A , Θ and P , to calculate their neutral tracer gradients. The local method is problematic in regions of weak vertical stratification, consequently requiring a variety of ad-hoc regularization methods that can lead to rather nonphysical dependencies for the resulting neutral tracer gradients. To avoid such dependencies Groeskamp et al. (2019a) developed the "vertical nonlocal method" (VENM), which is a search algorithm that requires no ad-hoc regularization and significantly improves the numerical accuracy of estimates of neutral slopes and gradients, making it one of the most accurate methods available for calculating neutral slopes and gradients from ocean observations. To the author's knowledge, the only model to date that has implemented a method comparable to VENM, is the Modular Ocean Model Version 6 (MOM6, (Adcroft et al., 2019)) by Shao et al. (2020). The results presented in this study, use the VENM method. However, to calculate the non-neutrality term, the results from the VENM algorithm are considered "perfectly neutral" in Eq. 14, while using the results from the local method as "ntr". VENM is not perfectly neutral, therefore the magnitude of the non-neutrality term is interpreted as an order of magnitude estimate of how much impact different methods of calculating neutral slopes and gradients can have on GMSL rise.

3.4 Velocity and surface height gradients

To calculate the ocean geostrophic velocity the TEOS-10 software 'gsw_geo_stf_dyn_height' is used to calculate the dynamic height anomaly streamfunction using the thermal wind balance. The derivatives of the streamfunction provide the associated geostrophic velocities using the function 'gsw_geostrophic_velocity' (McDougall and Barker, 2011). The 1000 dbar is used as reference level, with the associated reference level velocity taken from the YoMaHa'07 Argo float trajectories based estimates at 1000 db (Lebedev et al., 2007).

Sea surface height variation (η , as in Eq. 6) and gradients are estimated using 10 years (from 2014 to 2023) of altimeter satellite based Global Ocean Gridded L4 Sea Surface Height data, provided by E.U. Copernicus Marine Service Information (CMEMS).

265 3.5 Boundary mass and heat fluxes

Surface mass fluxes and air-sea-ice interaction are obtained from two products described below. The first product is the Objectively Analyzed air-sea Heat Fluxes (OA; Yu et al. (2008); Yu and Weller (2007)). The OA flux is constructed from optimal blending of satellite retrievals and three atmospheric reanalysis in combination with bulk formula. OA is combined with surface radiation data from the International Satellite Cloud Climatology Project (Zhang et al., 1995, 2004, 2007) to provide the heat
270 fluxes and evaporation from 1983–2006. Precipitation data accompanying the OA are obtained as the long-term (1981–2010) monthly means (2.5 degree grid) from the Global Precipitation Climatology Project Version 2.3 (Adler et al., 2003) and interpolated to the WOA grid. Runoff is obtained from time series (1900–2014) of monthly river flow from stations of the world’s largest 925 rivers, which excludes contributions from Greenland and Antarctica (Dai, 2016). Long-term monthly means are calculated, and 50% of the outflow to the ocean is allocated at the river mouth, spreading the other 50% over the grid points
275 directly surrounding the river mouth. The runoff data set does not take into account unmeasured continental runoff and underground seepage, which could be of the same order of magnitude as the river runoff but distributed over all global basins (Large and Yeager, 2004).

The second product is version 2 of Common Ocean Reference Experiment (CORE)-based product (Large and Yeager, 2009; Yeager and Large, 2008; Danabasoglu et al., 2014). Here bulk formula are applied in combination with adjusted wind speed
280 and humidity to decrease a global net imbalance from 30 W m^{-2} to 2 W m^{-2} . CORE combines the Global Precipitation Climatology Project with other products to obtain their precipitation (P) values. Monthly mean values (1949–2006) are constructed for latent heat, sensible heat, longwave radiation and shortwave radiation, evaporation and precipitation. Then a standard year is constructed by averaging for each calendar month for the WOA grid. Runoff is based on (Dai, 2016), but with an extra runoff term that is added for Antarctica.

285 Here the OA and CORE flux are chosen because they have the largest (OA, about 30 W m^{-2}) and smallest (CORE, about 2 W m^{-2}) globally integrated net heat flux imbalance (see Fig. 2 Valdivieso et al. (2017)). That makes them suitable to quantify the impact that different heat flux products have on GMSL budgets. Both mass flux products may inadequately represent barystatic contributions to sea level (included in R or I). For the OA flux is has to be part of the runoff term, through river discharge, while CORE has added extra mass flux from Antarctica that is not included in OA. This study does not examine the details
290 of the mass or heat flux products, and will only provide the impact on sea level that different products have. This will allow contrast and compare the magnitude of uncertainties between mass or heat flux estimates relative to other non-Boussinesq effects. In the next subsection it is discussed how these products are adapted to be globally balanced. The geothermal heat flux product is given by de Lavergne et al. (2015), based on Goutorbe et al. (2011).

3.5.1 Balanced boundary mass and heat fluxes

295 To quantify nonlinear thermal expansion, this study uses an artificially balanced mass and heat flux product that is applied to the 'standard year' climatology. This means that there is no net global heat flux that leads to climate change induced sea level rise, or GMSL rise due to land-ice melt. The exact procedure is given in Appendix E, but the overarching idea is that the total global imbalance is redistributed over each grid point for all contributing fluxes, and proportional to the magnitude of the local flux. This assumes that if at a given time and location the flux is large, that the error is also larger and it can compensate a larger
300 proportion of the total imbalance. The result is a global net-zero mass and heat flux. This method is applied to both mass and heat fluxes of OA and CORE and referred to as the "balanced" products.

3.6 Shortwave radiation (SWR) depth penetration parameterization

SWR that reaches the surface of the ocean, is redistributed with depth using a structure function $F(z)$ (see Eq. B4). The vertical distribution of the SWR will lead to density changes over a range of depths, instead of only at the surface (Iudicone et al., 2011; Groeskamp and Iudicone, 2018). $F(z)$ can depend on factors such as water clarity and chlorophyll concentrations (Lewis et al., 1990; Morel and Antoine, 1994; Ohlmann, 2003). This study compares the impact on GMSL rise, using three different SWR depth penetration parameterizations that are detailed in Eq. B7 in Appendix B. The general results that are presented in this study and in particular in Table 2 use the parameterization F_{MA94} from Morel and Antoine (1994) (Eq. B7). Differences with other parameterizations are discussed in section 4.4. Because F_{MA94} depends on chlorophyll-a, a chlorophyll-a climatology is
310 constructed (similar to that done in Groeskamp and Iudicone (2018)). This is based on a 9-km resolution monthly mean Sea-viewing Wide Field-of-view Sensor data. Data for the period 1997–2010 is used (Hu et al., 2012), which is spatially averaged to the WOA climatology, and subsequently time averaging for each calendar month. This process provides a standard year of monthly means that should be a good first-order estimate of the decay factors in F_{MA94} for the purposes of this paper.

4 Results

315 This section discusses the results of the quantification of local sea level evolution and GMSL rise due to the different processes described in section 2, in combination with the data described in section 3. The results are presented as spatial maps of sea level rise in mm year^{-1} , and their global integrals. The given numbers for sea level rise and GMSL rise represent annual mean values, based on a standard year (see section 3).

4.1 GMSL rise due to mass fluxes

320 Here the direct impact of ocean mass fluxes on sea level rise is discussed (section 2.1, Eq. 4). The indirect impact of mass fluxes on the salinity budget (Eq. 5) are discussed in section 4.2. The largest contributions to GMSL is due to Precipitation P (just over $1100 \text{ mm year}^{-1}$) and evaporation E (just below $-1100 \text{ mm year}^{-1}$), and are of opposite sign. Some precipitation falls on land and enters back via river runoff, which is why precipitation is a bit smaller than evaporation and the difference is about the

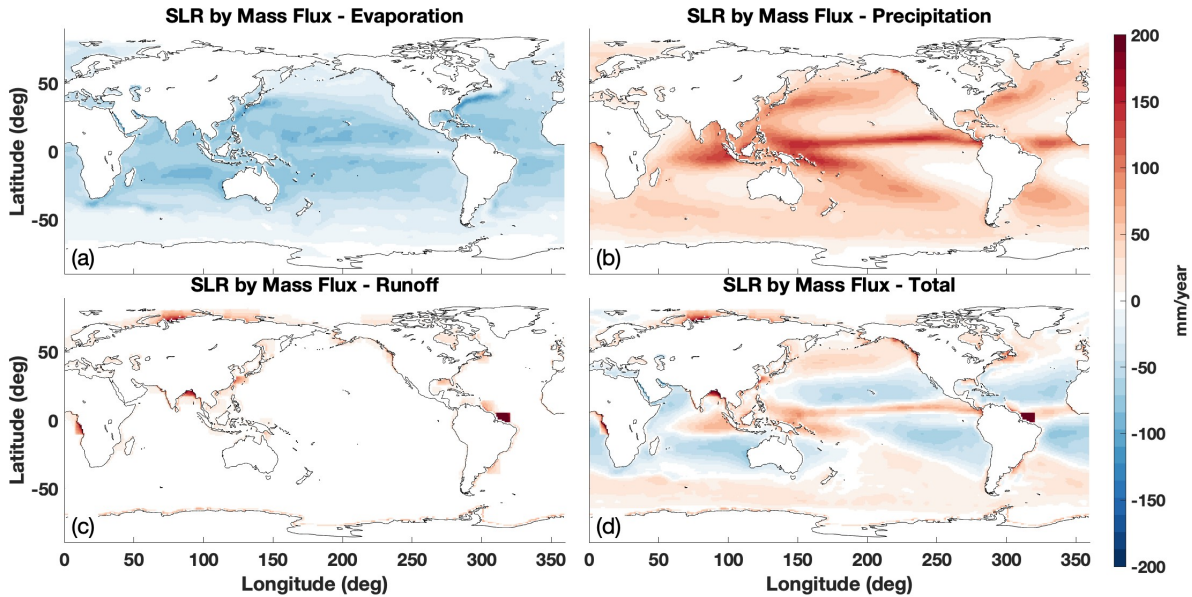


Figure 1. The spatial impact of mass fluxes on sea level rise (mm year^{-1}) due to Evaporation (a), Precipitation (b), Runoff (c) and their sum (d) for the CORE dataset. Derivations and discussion of these terms are found in sections 2.1, 3.5, 4.1, Eq. 4 and Table 2.

same as that from river runoff and of the order of $65\text{--}85 \text{ mm year}^{-1}$ (Table 2). The different impact on GMSL between CORE and OA due to E , R and P is 65 , 19 and 7 mm year^{-1} , respectively. For R this is probably related to Antarctic runoff added in the CORE product that is not included in OA. For E and P such differences may arise from different bulk transfer algorithms, calibration protocols and reason for which a product is designed. The total difference in GMSL rise between CORE and OA is about 40 mm year^{-1} , ten times the observed rates of current sea level rise. This means that uncertainties between the products, also swamp the impact of poorly represented barystatic sea level changes of approximately 2 mm year^{-1} . This clearly indicates the difficulty to accurately represent mass fluxes into the ocean and the impact this could have on sea level rise calculations.

Resulting spatial patterns of sea level evolution due to E , P and R are a direct reflection of well-known evaporation, precipitation and runoff patterns (Fig. 1). Sea level decreases in subtropical regions where evaporation dominates, while sea level increases at higher latitudes and equatorial regions where precipitation dominates (Fig. 1d).

When examining the GMSL changes due to the constructed balanced mass flux products of CORE and OA (section 3.5.1 and Appendix E), the net change in GMSL is of the order of 0.1 mm year^{-1} , similar to that found by (Griffies and Greatbatch, 2012) in a numerical model. This is a consequence of mass entering the ocean at higher densities (higher latitudes), while leaving the ocean at lower densities (lower latitudes, Eq. 1).

GMSL in mm year ⁻¹	Normal		Balanced	
	CORE	OA	Core	OA
Total Mass	-35	3.3	0.11	0.05
Evaporation	-1185	-1120	-1167	-1121
Precipitation	1064	1057	1080	1055
Runoff	85	66	87	66
Total Freshwater	-1.2	-0.24	-0.27	-0.33
Evaporation	-30	-29	-30	-29
Precipitation	27	27	28	27
Runoff	2.1	1.5	2.1	1.5
Total Heat	13	57	5.8	1.0
Longwave	-99	-92	-101	-100
Shortwave	339	356	335	326
Latent heat	-203	-189	-205	-205
Sensible heat	-23	-18	-24	-19

Table 2. Area weighted GMSL rise in mm year⁻¹, calculated using Eq. 2 for surface mass fluxes (first 4 rows), freshwater fluxes (row 5-8) and heat fluxes (row 10-14). Mass and freshwater fluxes are due to evaporation, precipitation, and runoff, while heat fluxes include radiative fluxes (longwave and shortwave) and turbulent fluxes of latent heat and sensible heat. Bold indicate their sums. See also sections 2.2, 4.1-4.3, Eq. 4, 5 and Figs. 1, 2 and 3.

4.2 GMSL rise due to the surface freshwater flux

The mass flux (Eq. 3) is also a freshwater flux (Eq. B1) that can be converted into an equivalent salt-flux that alters salinity and thereby density and sea level (section 2.2, Huang (1993); Nurser and Griffies (2019); Groeskamp et al. (2019b)). The difference between the mass flux and salt flux is only a factor βS_A , meaning that the impact of the salt fluxes on local and GMSL rise is almost 40 times smaller than the direct impact of the individual mass flux terms (Table 2). The impact on GMSL rise due to freshening resulting from precipitation is about 27 mm year⁻¹, a bit smaller than the impact from evaporation of about -30 mm year⁻¹ (Table 2). The residual is covered by the impact on freshening by river runoff (about 2 mm year⁻¹). Resulting patterns of sea level evolution are different from E , P and R by the factor βS_A , but overall comparable (Fig. 2). Hence, as for the mass flux, sea level decreases in subtropical regions where evaporation dominates, while sea level increases at higher latitudes and equatorial regions where precipitation dominates (Fig. 2d).

The net impact of freshwater fluxes is about -1 mm year⁻¹, with the difference between OA and CORE being about the same size and thus of the same order as observed GMSL rise. As for the balanced mass flux products, the resulting "nonlinear haline expansion" leads to a GMSL change of about -0.3 mm year⁻¹ for both products, which is of the same order of magnitude as found by Griffies and Greatbatch (2012). This is nonzero as the balanced mass flux is weighted by the factor βS_A , which leads to a net GMSL rise that is non-negligible, but almost an order of magnitude smaller than observed GMSL rise.

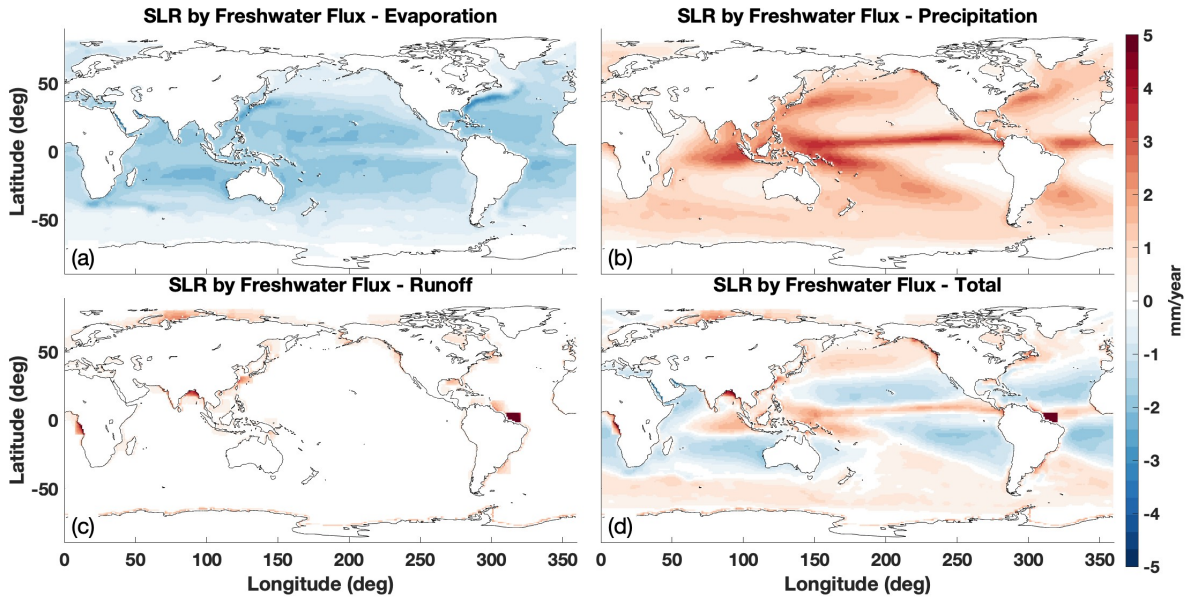


Figure 2. The spatial impact of freshwater fluxes on sea level rise (mm year^{-1}) due to Evaporation (a), Precipitation (b), Runoff (c) and their sum (d). Results are shown for the CORE dataset. Derivations and discussion of these terms are found in sections 2.2, 3.5, 4.2, Eq. 5 and Table 2.

4.3 GMSL rise due to the surface heat flux

This section presents the effect of the sensible heat flux, latent heat flux, and long-wave heat flux that are exchanged at the oceans surface on local and GMSL rise (section 2.2). Also, the impact on GMSL rise due to shortwave radiative heat flux is presented, that may penetrate deeper into the ocean (section 3.6, Table 2 and Fig. 3). The shortwave heat flux leads to an increase in sea level, where the other heat fluxes lead to a decrease. Their individual impacts on GMSL vary from $-200 \text{ mm year}^{-1}$ to 350 mm year^{-1} (Table 2). The total net impact of heat flux is about $10\text{-}50 \text{ mm year}^{-1}$, i.e. with a difference between the two products of about 40 mm year^{-1} , comparable to that due to global mass fluxes. This difference is not unexpected as heat flux products are notoriously difficult to close (Josey et al., 1999; Yu, 2019). A net global heat flux of 0.3 W m^{-2} is enough to explain the observed increase in global heat content (Domingues et al., 2008; Ishii and Kimoto, 2009; Levitus et al., 2012; Lyman and Johnson, 2013), while imbalances up to 30 W m^{-2} are not uncommon for available heat flux products (Balmaseda et al., 2015; Valdivieso et al., 2017). The CORE and OA flux products have some of the largest difference in net heat flux (Valdivieso et al., 2017), meaning that these results should be a good indication of the range that can be expected from the impact of heat fluxes on GMSL.

Resulting patterns of sea level evolution (Fig. 3) are a direct reflection of heat flux patterns themselves that can be found in many different studies (Josey et al., 1999; Yu, 2019; Tang et al., 2024). Of interest is the distribution of these fluxes, showing warming around the equator and cooling at western boundary currents and higher latitudes (Fig. 3e). As the thermal expansion

coefficient can vary up to a factor of 10 (especially with latitude), this leads to differently weighted impact of warming and
370 cooling on sea level.

Nonlinear thermal expansion is calculated using the balanced heat flux products (so no expansion due to net warming, see
section 3.5.1) and estimated to be 1 - 6 mm year⁻¹. This is comparable to the 10 mm year⁻¹ found by Griffies and Greatbatch
(2012) (their Fig. 7). Hence, both the magnitude of the nonlinear thermal expansion, as well as the difference between the
products, is of the same order as the observed GMSL rise (4 mm year⁻¹). The differences are related to different emphases
375 between products in which heat leaves or enters the ocean, demonstrating the importance of carefully constructing heat flux
products. Note that the impacts from both the nonlinear haline contraction and mass fluxes are about an order of magnitude
smaller than those from nonlinear thermal expansion (Table 2). In section 4.6 the balance between densification upon mixing
and nonlinear thermal and haline expansion is examined.

4.4 GMSL rise due to different SWR penetration parameterizations

380 The total incoming SWR at the surface is vertically redistributed according to some vertical structure function $F(z)$ (section
2.2, or Eq. B8). This means that a part of the heat reaching the surface is actually accumulating and transforming water below
the surface. Most often sub-surface temperatures will be cooler with a smaller thermal expansion coefficient α , and thus a net
smaller volume increase compared to the hypothetical situation in which all SWR is absorbed at the surface. The results in row
11 of Table 2 were computed using the vertical distribution function of Morel and Antoine (1994) (Eq. B7). When the other
385 two specified functions (section 4.4) are applied to the balanced products for CORE, the observed change in GMSL due to the
total heat flux is 4.7, 5.8, and 6.7 mm year⁻¹ for F_{PS77} , F_{MA94} (as above) and F_{SF} , respectively. Taking the balanced products
for OA, this gives -0.05, 1.0 and 2.0 mm year⁻¹ for F_{PS77} , F_{MA94} (as above) and F_{SF} , respectively. As F_{PS77} allows for the
deepest penetration, this will lead to the least increase, followed by F_{MA94} and F_{SF} . For the unbalanced heatflux products
the difference due to different SWR parameterizations are similar (not shown). In conclusion, GMSL rise can change 1.0 mm
390 year⁻¹, depending on the choice of SWR depth penetration parameterization.

4.5 GMSL rise due to geothermal heating

Geothermal heat injection from the sea floor leads to sea water expansion and local sea level rise. This predominantly occurs
along ocean ridges, with additional hot-spots in the Caribbean Sea and the waters around South East Asia (Fig. 4). The large
ocean basins have values that are an order of magnitude lower, but cover large surface areas. The total impact of geothermal
395 heating on GMSL is 0.08 mm year⁻¹. This is relatively small compared to other processes (Table 6) and is exactly similar to
that calculated in a numerical model (Griffies and Greatbatch, 2012) (their Table 1).

4.6 GMSL rise due to mixing

Here the impact on GMSL due to mixing processes is quantified (Section 2.3, Eq. 6). The impact on GMSL rise by both
constant diffusivities as well as the more realistic spatially varying diffusivities (section 3) are compared and contrasted. This

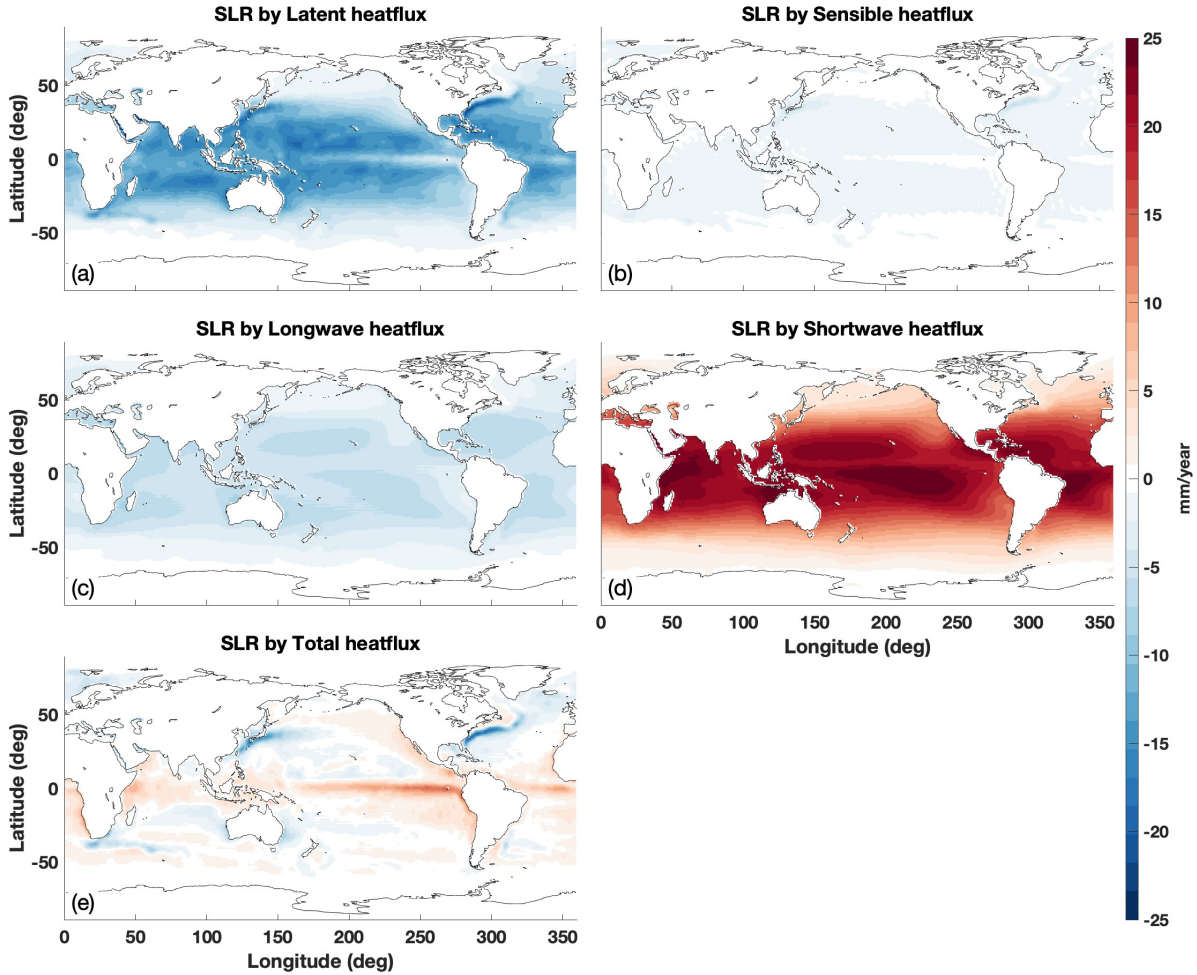


Figure 3. The spatial impact of heat fluxes on sea level rise (mm year^{-1}) due to latent heat flux (a), sensible heat flux (b), longwave heat flux (c), shortwave heat flux (d) and their sum (e). For SWR penetration the Morel and Antoine (1994) parameterization is used (Eq. B7). Derivations and discussion of these terms are found in sections 2.2, 3.5, 4.3, Eq. 5, and Table 2.

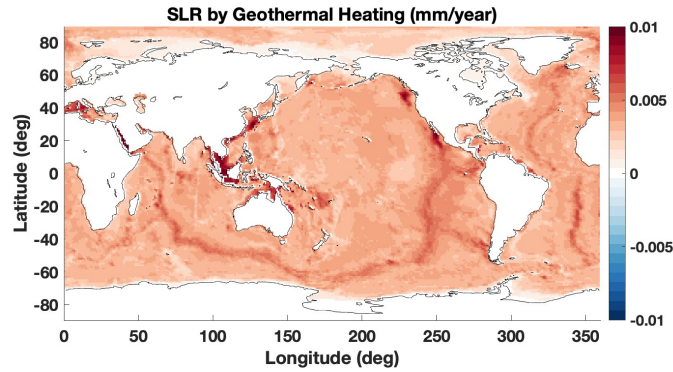


Figure 4. The spatial impact on sea level rise (mm year^{-1}) by geothermal heating, which is derived and discussed in sections 2.2, 3.5, 4.5, Eq. 5, and Table 6.

400 gauges the range of possible outcomes of the impact on GMSL rise due to using different mixing parameterizations. The results for a constant diffusivity are simply proportional to the diffusivity, and can therefore easily be rescaled with a different constant diffusivity in mind.

For variable diffusivities, the largest impact on GMSL is by vertical cabbeling (-2 mm year^{-1}), and to a lesser extent by horizontal ($-0.4 \text{ mm year}^{-1}$) and neutral cabbeling ($-0.5 \text{ mm year}^{-1}$). Together these processes are decreasing GMSL with
 405 a rate of about -3 mm year^{-1} (Table 3). Somewhat important are vertical thermobaricity (0.2 mm year^{-1}) and the bottom boundary condition term ($-0.1 \text{ mm year}^{-1}$). All other mixing-related terms have an almost negligible impact on GMSL rise (Table 3).

The use of a constant diffusivity is an overly simplistic alternative that instead might overestimate the impact of vertical mixing and results in $D_{\text{constant}} > D(x, y, z)$ in the upper 2500 meter of the ocean. This explains the difference of a factor 5 in
 410 GMSL rise due to vertical cabbeling, between using a variable or constant vertical diffusivity D . The best way to narrow down this estimate is to first include an observational-based estimate of a surface layer boundary mixing scheme, which is beyond the scope of this study.

Taken together, the total impact of all mixing on GMSL rise is between -3 and -11 mm year^{-1} . This indicates that both the impact of mixing itself, as well as the difference between mixing parameterizations, are of the same order as the observed
 415 GMSL rise. In addition, the impact of mixing is comparable in magnitude and of opposite sign to the impact from nonlinear thermal expansion (Table 2, section 4.3), suggesting that densification upon mixing can counteract expansion due to nonlinear thermal expansion.

Vertical cabbeling takes place where there is vertical mixing by internal waves (de Lavergne et al., 2020) in combination with vertical gradients of temperature and salinity (Eq. C22), which is mostly around topography (Fig. 5a). Although the integrated
 420 impact of vertical diffusion on GMSL rise is comparable to that found in Griffies and Greatbatch (2012), the spatial structure of this effect is very different (their figure 10a). The differences between these studies is best explained by the different diffusivity

Process:	Variable Diffusion	Constant Diffusion
Total (unit of mm year ⁻¹)	-2.8	-11
Cabbeling Vertical $P_{C_b}^{verr}$	-2.0	-10
Cabbeling Horizontal $P_{C_b}^{hor}$	-0.48	-0.75
Cabbeling Neutral $P_{C_b}^{ntr}$	-0.44	-0.41
Thermobaricity Vertical $P_{T_b}^{ver}$	0.16	0.49
Bottom Bdy-term $\mathbf{R}^{hor} \cdot \nabla_H(-H)$	-0.12	-9.0×10^{-2}
Thermobaricity Neutral $P_{T_b}^{ntr}$	-3.7×10^{-2}	-2.7×10^{-2}
$D^{-1} \mathbf{R}^{ver} ^2$ -term	-1.4×10^{-2}	-9.5×10^{-2}
$K_H^{-1} \mathbf{R}^{hor} ^2$ -term	-3.3×10^{-3}	-2.9×10^{-3}
$\rho g \kappa \mathbf{k} \cdot \mathbf{R}^{ver}$ -term	-6.0×10^{-3}	-2.3×10^{-2}
Surface Bdy-term $\mathbf{R}^{hor} \cdot \nabla_H(\eta)$	-2.5×10^{-5}	-3.7×10^{-5}
Thermobaricity Horizontal $P_{T_b}^{hor}$	1.5×10^{-5}	2.2×10^{-5}

Table 3. Area weighted GMSL rise in mm year⁻¹, calculated using Eq. 2 for different mixing terms as described in section 2.3 and Eq. 6 and shown in Figs. 5 and 6.

parameterizations. Vertical thermobaricity is of opposite sign to cabbeling and smaller, this increasing sea level at locations where vertical cabbeling is also strong (Fig. 5d).

Neutral temperature and salinity gradients are particularly strong in the Southern Ocean at mid-depths, near western boundary currents and to a lesser extent in the major ocean basins (Groeskamp et al., 2019a). The mesoscale diffusivity are particularly strong near western boundary currents and in some of the subtropical regions (Groeskamp et al., 2020). Together this means the impact of neutral cabbeling on sea level rise is mostly centered around western boundary currents and to some extent in the Southern Ocean (Fig. 5c). This is expected, as other studies also found these location to be a hotspot for neutral cabbeling (Groeskamp et al., 2016; Klocker and McDougall, 2010; Griffies and Greatbatch, 2012; Urakawa and Hasumi, 2012). For similar reasons, neutral thermobaricity is large in many of the same places as neutral cabbeling, but is generally smaller and can lead to both sea level rise and fall (Fig. 5e). Horizontal cabbeling is defined using the same diffusivity as neutral mixing, but only in the mixed layer. This means it is more pronounced where mixed layers are also deeper (Fig. 5b), such as in the Southern Ocean and the North Atlantic (de Boyer Montégut et al., 2004).

Overall mixing decreases sea level (Fig. 5f), with the largest impact where the different cabbeling processes are strong. The spatial distribution of the small (negligible) terms are shown for completeness (Fig. 6), but not further discussed.

4.7 GMSL rise due to stirring

The impact of stirring on sea level (section 2.4, Eq. 11) is investigated by comparing results using a constant mesoscale diffusivity to those using a spatially varying mesoscale diffusivity (section 3.2). There are only three terms contributing to stirring, of which the first term is zero after global integration (Eq. 11). Of the remaining two terms, the production term P_{stir}

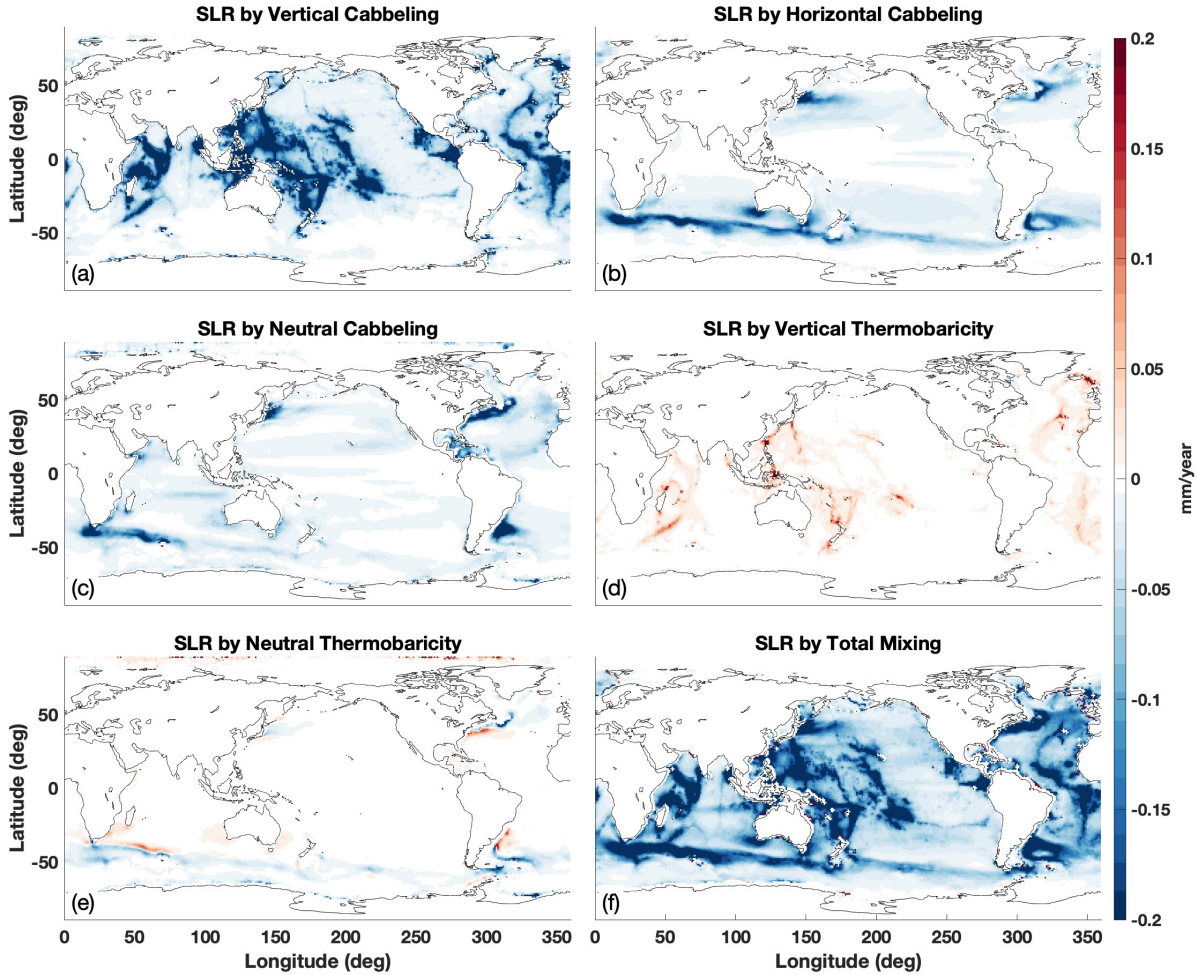


Figure 5. The spatial impact on sea level rise (mm year^{-1}) by the most important mixing terms, due to vertical cabbeling (a), horizontal cabbeling (b), neutral cabbeling (c), vertical thermobaricity (d), Neutral Thermobaricity (e) and the sum of all mixing terms (f), including the ones shown in Fig. 6. The mixing terms are derived and discussed in sections 2.3, 3.2, 4.6, Eq. 6, and Table 3.

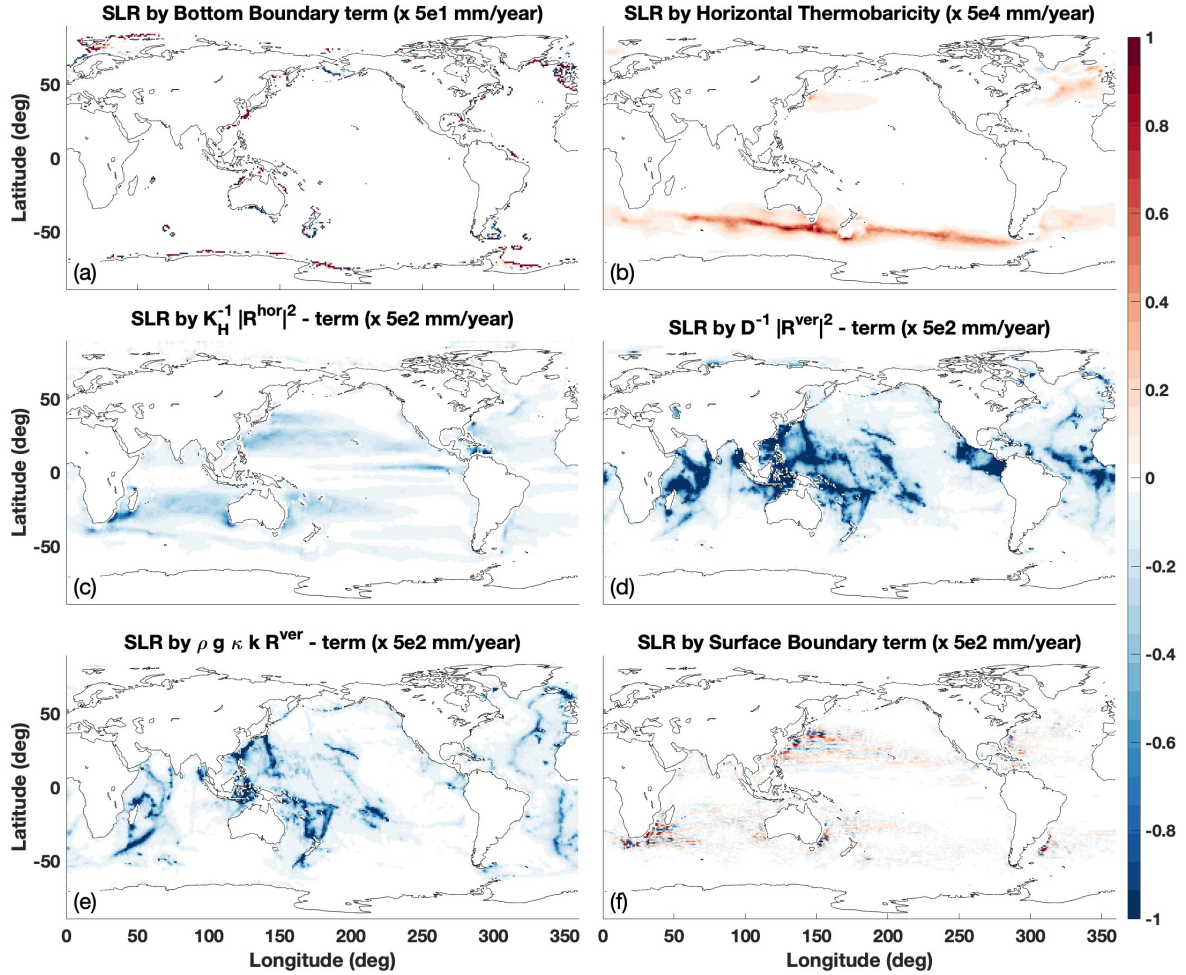


Figure 6. The spatial impact on sea level rise (mm year^{-1}) by the mixing terms with a small impact. Shown are the bottom boundary term (a), horizontal thermobaricity (b), diffusion-density interaction with horizontal mixing $K_H^{-1} |\mathbf{R}^{\text{hor}}|^2$ -term (c), the diffusion-density interaction with vertical mixing $D^{-1} |\mathbf{R}^{\text{ver}}|^2$ -term (d), diffusion-density interaction with horizontal mixing $\rho g \kappa k \cdot \mathbf{R}^{\text{ver}}$ -term (e), and the surface Boundary term $\mathbf{R}^{\text{hor}} \cdot \nabla_H(\eta)$ (f). Note the multiplication factor given in the title, which is used for all terms to have the same color-scale. The mixing terms are derived and discussed in sections 2.3, 3.2, 4.6, Eq. 6, and Table 3.

Process	Variable Diffusion mm year ⁻¹	Constant Diffusion mm year ⁻¹
Total	-0.55	-0.36
Production by Stirring P_{stir}	-0.53	-0.35
$\mathbf{R}^{\text{stir}} \cdot \nabla \ln \rho$ -term	-1.4×10^{-2}	-9.1×10^{-3}

Table 4. Area weighted GMSL rise in mm year⁻¹, calculated using Eq. 2 for stirring. See also sections 2.4, 4.7, Eq. 11 and Fig. 7.

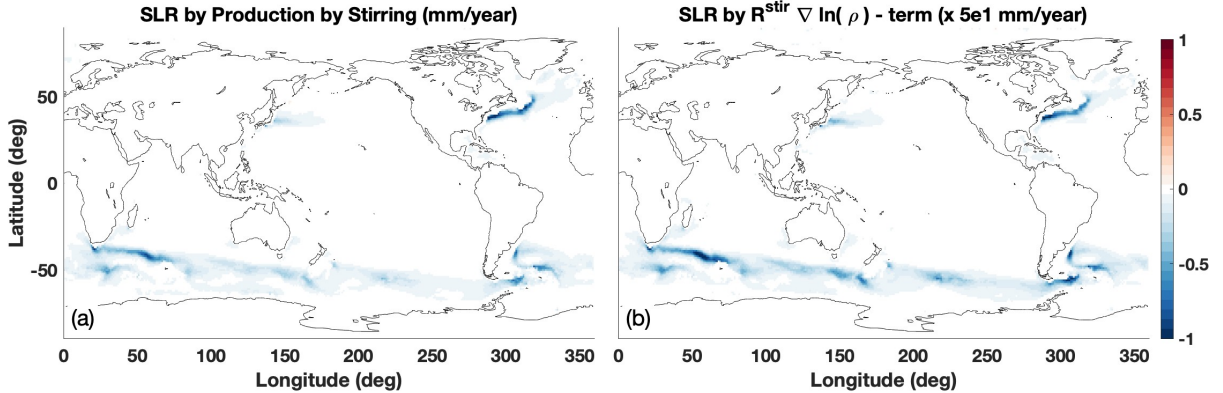


Figure 7. The spatial impact of the stirring terms on sea level rise (mm year⁻¹), due to stirring production term (a) and the $\mathbf{R}^{\text{stir}} \cdot \nabla \ln \rho$ -term (b). Note the multiplication factor given in the title of panel b. The stirring terms are derived and discussed in sections 2.4, 3.2, 4.7, Eq. 11, and Table 4.

440 has a non negligible impact on GMSL rise of about -0.4 to -0.6 mm year⁻¹ (Table 4), that is about 8 times smaller than observed GMSL rise.

The stirring parameterization includes a factor $K S$ (Eq. D6), causing the main impact on sea level to be where the combination of both neutral slopes and mesoscale diffusivity are large. This is between 40°S and 50°S and in western boundary currents (Fig. 7). Although its global mean impact is moderate, it could locally be important.

445 4.8 GMSL rise due to Non-Neutrality

Here the impact of non-neutrality on GMSL is quantified (Section 2.5, Eq. 14). As explained in section 3.3, two methods are used for calculating neutral slopes and gradients. The results from the VENM algorithm is used as perfectly neutral in Eq. 14, while using the results from the local method as ntr. As VENM is not perfectly neutral, the results should be interpret as the order of magnitude of the improvement that can be made when accurate neutral physics is implemented.

450 The first (non-divergent) term in Eq. 14 has no net contribution to GMSL rise by construction and is discussed in section 4.9. The three non-neutral terms that are related to \mathbf{R}^{ntr} (Eq. 14), all have very small contribution to GMSL (Table 5, Fig. 8c,d,e). Note these can be directly calculated using the gradients obtained from the VENM method, and these terms would be larger

Process	Variable Diffusion mm year ⁻¹	Constant Diffusion mm year ⁻¹
Total	-2.7	-2.4
$P^{\text{ntnr}} - P^{\text{(perfectly neutral)}}$	-2.5	-2.2
$\frac{\partial \eta}{\partial t} \Big _{\text{stirring}}^{\text{non-neutral}}$ -term	-0.16	-0.13
Bottom Bdy-term $\mathbf{R}^{\text{ntnr}} \cdot \nabla_{\text{H}}(-H)$	-7.4×10^{-4}	-4.4×10^{-2}
$\kappa \nabla_{\text{N}} P \cdot \mathbf{R}^{\text{ntnr}}$ -term	1.8×10^{-5}	6.4×10^{-5}
$K_{\text{N}}^{-1} \mathbf{R}^{\text{ntnr}} ^2$ -term	-1.1×10^{-6}	-5.5×10^{-6}

Table 5. Area weighted GMSL rise in mm year⁻¹, calculated using Eq. 2 for non-neutral terms. See also sections 2.5, 4.8, Eq. 14 and Fig. 8.

when using the local method as that is much less neutral and more irregular (Groeskamp et al., 2019a). However, these terms are small, even when using the local method, and are not further discussed.

455 The main impact of non-neutrality to GMSL rise comes from the neutral cabbeling and thermobaricity terms (-2.5 mm year⁻¹), and to a lesser extent from eddy stirring (-0.2 mm year⁻¹). The impact of calculating these terms using different methods is in total about -3 mm year⁻¹, with a small impact from the difference in diffusivity. This means that the use of the local method makes an error of at least the same order of magnitude as observed GMSL rise rates themselves.

4.9 GMSL redistribution terms

460 The four redistribution terms that have local impact on sea level, but no net impact on GMSL, are from ocean currents (Eq. 10, section 2.4), from horizontal diffusion (Eq. 6, section 2.3), from neutral diffusion (a non-neutrality term, Eq. 14, section 2.5) and from stirring (Eq. 11, section 2.4). The redistribution terms have a large impact on local sea level rise (except the neutral term). The largest impact on local sea level is by dynamical sea level changes (Fig. 9d). In all cases, clear patterns of positive and negative change exist due to the divergence operator (Fig. 9). The shape and location of these patterns are related to specific
465 processes. For example; the horizontal diffusion redistributes volume from the subtropics to the equator, while stirring does this within western boundary currents. Overall these results are not further examined, but the figures are provided for completeness.

5 Summary and Discussion

Observation-based mass and heat fluxes are by far the largest contributors to GMSL changes, but they are notoriously hard to balance due to a lack of observational constraints. For example, the GMSL rise estimates based on the mass flux (-35 to 3 mm
470 year⁻¹, Table 6) or the heat flux (13 to 57 mm year⁻¹, Table 6) are both about ten times larger than the observed GMSL rise (4 mm year⁻¹). For comparison, Griffies and Greatbatch (2012) found the net impact of the ocean mass flux on sea level to be 0.8 mm year⁻¹ in a numerical model environment (their Fig. 2). The impact on GMSL rise estimated from different heat and mass fluxes is also about ten times larger than the observed GMSL rise. The main source of these differences for mass flux products is the representation of ocean evaporation and precipitation processes (Section 4.1 and Table 6), which overwhelm

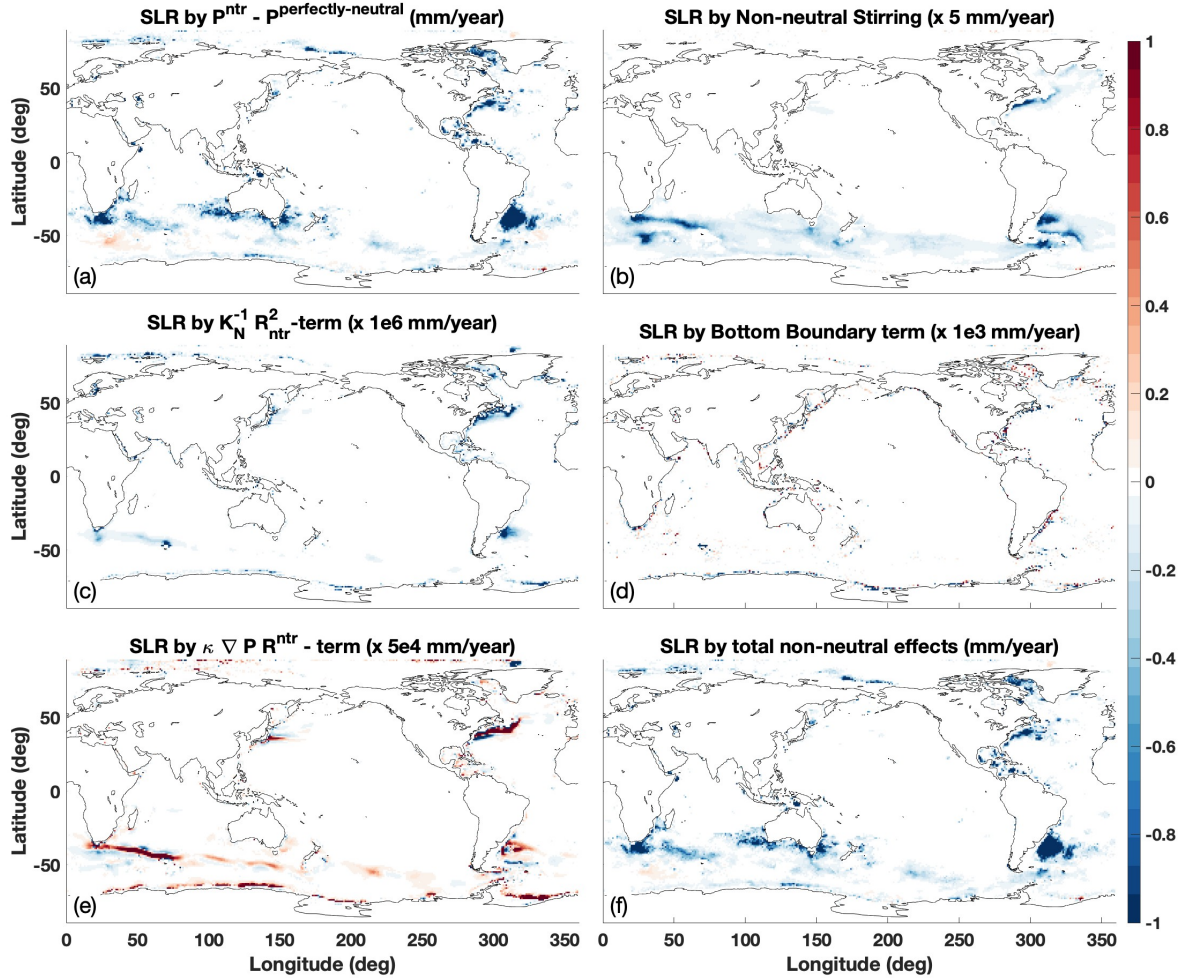


Figure 8. The spatial impact of the non-neutral terms on sea level rise (mm year^{-1}), due to the production terms (a), the stirring production term (b), the $K_N^{-1} |\mathbf{R}^{\text{ntr}}|^2$ -term (c), the bottom boundary term (d), the $\kappa \nabla_N P \cdot \mathbf{R}^{\text{ntr}}$ -term (e), and the sum of all these terms (f). Note the multiplication factor given in some of the titles, which is used for all terms to have the same color-scale. The non-neutral terms are derived and discussed in sections 2.5, 3.3, 4.8, Eq. 14, and Table 5.

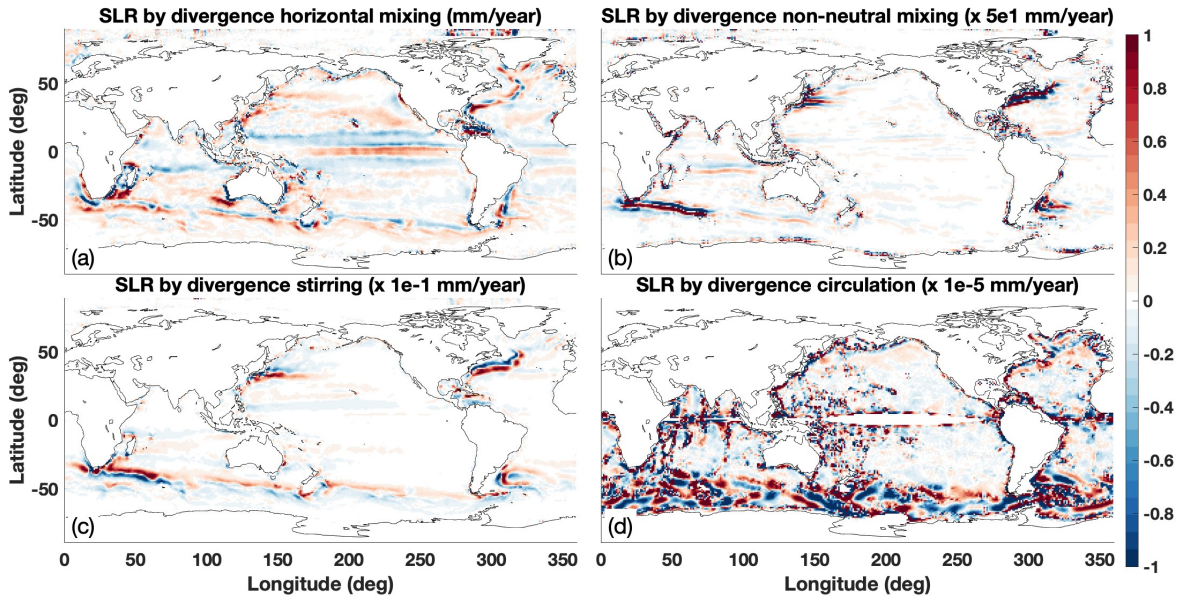


Figure 9. The spatial impact of the redistribution terms on sea level rise (mm year^{-1}), due to horizontal mixing divergence (a), non-neutral divergence (b), stirring divergence (c) and ocean dynamics (d). Note the multiplication factor given in the titles, which is used for all terms to have the same color-scale. The divergence terms are discussed in section 4.9.

Process	mm year^{-1}	
Mass [balanced product]	-35 to 3	[0.05 to 0.1]
Heat [balanced product]	13 to 57	[1 to 6]
Fresh water [balanced product]	-0.2 to -1.2	[-0.3]
Diffusion	-11 to -3	
Stirring	-0.6 to -0.4	
Non-neutrality	-3	
Shortwave radiation parameterization	± 1	
Geothermal Heating	0.08	

Table 6. Summary of the area weighted GMSL rise in mm year^{-1} for the different processes discussed in this paper. The results from the balances mass and heat flux product are given in brackets.

475 uncertainties in the representation of barystatic sea level rise. Similarly, different bulk formulas and choices in calculating heat fluxes may have a large impact on GMSL rise. Improving the mass and heat flux products is beyond the scope of this study. This study only gauges the magnitude of their impact and uncertainties. With such large inaccuracies in estimating GMSL rise, it is not yet possible to close the GMSL budget using the sum of the contributing processes, i.e., the bottom-up approach.

Therefore, this study also uses heat and mass flux products that are artificially forced to have a globally integrated net-zero
480 mass and heat flux (Appendix E). This approach is somewhat comparable to numerical ocean models that remove global mass
imbalances at each time step to prevent long-term drift (Griffies, 2012). For the balanced mass fluxes, the impact on GMSL is
about 0.1 mm year^{-1} . The residual is a consequence of nonlinear weighting of the mass fluxes by the ocean surface density
(Eq. 4). The mass flux can also be recalculated into an equivalent salt flux (using the factor βS_A , Eq. B8), which affects density
and changes GMSL by about $-0.3 \text{ mm year}^{-1}$.

485 The impact of balanced heat flux products on GMSL is reduced by an order of magnitude compared to the unbalanced
products to $1\text{-}6 \text{ mm year}^{-1}$. This is not due to "regular" thermal expansion from climate change warming, as there is net-
zero heat going into the ocean. Instead this is due to nonlinear thermal expansion as a consequence of the heat fluxes being
weighted by the thermal expansion coefficient that varies strongly with temperature, before global integration (Eq. B8). Note
that (slight) differences in spatial variation between the two heat flux products, lead to a difference in GMSL rise estimate of 5
490 mm year^{-1} . Hence, both the value and the uncertainty in calculating the nonlinear thermal expansion are of similar magnitude
as the observed GMSL rise of 4 mm year^{-1} .

The combination of horizontal, neutral, and vertical mixing leads to densification upon mixing and subsequent reduction
in GMSL of -3 to -11 mm year^{-1} . This is mostly due to vertical mixing, and to a lesser extent due to horizontal and neutral
mixing. Griffies and Greatbatch (2012) found that the KPP-mixing scheme for the surface boundary layer (Large et al., 1994;
495 Van Roekel et al., 2018) has a comparable impact on GMSL rise as vertical mixing over the entire ocean. The small-scale
diffusivities used in this study (de Lavergne et al., 2019) to estimate the impact of vertical mixing on GMSL rise do not include
surface boundary layer parameterizations and therefore underestimate surface boundary layer mixing processes. The impact of
vertical mixing could therefore be underestimated by about a factor of 2. Note that thermobaricity, a nonlinear effect related
to pressure and temperature changes, can lead to both a sea level rise and fall. However, this term is in general an order of
500 magnitude smaller than the impact of densification upon mixing. The range of the impact of mixing on GMSL rise depends
mostly on the parameterizations used for mixing diffusivity (mixing strength).

It is concluded here that (1) mixing itself has a first-order effect on GMSL rise, and (2) differences between mixing strength
parameterizations have an impact on GMSL of the same order as the observed GMSL rise. This means that mixing matters for
GMSL. This is of interest for numerical modeling purposes because mixing parameterizations can vary strongly between mod-
505 els (Pradal and Gnanadesikan, 2014), thereby differently impacting GMSL rise budgets. Stirring of heat and salt by mesoscale
eddies decreases GMSL rise at a rate of -0.4 to $-0.6 \text{ mm year}^{-1}$, which is important but smaller than the impact of diffusion.

In this study, both nonlinear thermal expansion and densification upon mixing are separately quantified and are, within the
range of the estimates, indeed of the same order of magnitude but of opposite sign. Note that if the ocean were of uniform
temperature and salinity, both effects would not exist. Hence, these two processes will always occur together: as heat fluxes
510 create extremes and induce nonlinear thermal expansion, mixing acts to homogenize the ocean, causing densification upon
mixing. As models include choices about mixing parameterizations and boundary flux products, this leads to some balance
between nonlinear thermal expansion and densification upon mixing. It is complex to understand what impact these choices
have on the GMSL budgets and related predictions of future sea level rise. In addition, the time scales related to the impact of

densification upon mixing and nonlinear thermal expansion are likely very different, implying a time lag between the effects of
515 these two processes. Understanding this interplay is of interest but beyond the scope of this study. This study thus emphasizes
the importance of ocean mixing, not only for circulation (de Lavergne et al., 2022; Holmes et al., 2022), climate (Melet et al.,
2022) and biogeochemical processes (Lévy et al., 2022; Spingys et al., 2021), but also for sea level rise (Gille, 2004; Jayne
et al., 2004).

This study shows that the way neutral physics is implemented, has a first order effect on GMSL rise. Incorrect implementa-
520 tion of neutral physics leads to additional mixing and related densification upon mixing. Differences in neutral physics methods
used to calculate neutral slopes and gradients lead to a GMSL difference of about -3 mm year^{-1} , which is a leading-order term.
This results in a low bias, something also hinted at by Gille (2004) in a numerical model. This emphasizes the need to integrate
the most advanced and accurate methods for neutral physics calculation in numerical models for predicting future sea level rise
(Groeskamp et al., 2019a; Shao et al., 2020).

525 Different ways of parameterizing the vertical distribution of shortwave radiation cause differences in which water layers are
heated. Parameterizations that allow for deeper penetration heat colder waters. As colder water has a lower thermal expansion
coefficient, heating cold water leads to less sea level rise than heating warm water. Parameterizations that allow deeper
penetration of shortwave radiation will thus have a smaller impact on GMSL rise. Differences in sea level rise between such
parameterizations lead to GMSL rise differences of about $\pm 1 \text{ mm year}^{-1}$. Not only is this a large term, but the effect is
530 unidirectional over time and has the potential to accumulate to 10 cm per century.

6 Conclusions

The sum of barystatic and steric sea level change can explain the observed GMSL rise as derived from tide gauges and satellite
altimetry (Moore et al., 2011; Horwath et al., 2022; Frederikse et al., 2020; Church et al., 2011; Ludwigsen et al., 2024;
Frederikse et al., 2020). The calculations and methods involved in obtaining the steric and barystatic estimates are derived
535 from large top-down integrals of ocean hydrographies and satellite observations. However, this top-down approach glosses
over the impact on the GMSL budget of individual physical oceanographic processes. This study therefore applied a bottom-
up approach in which the contributions of individual physical processes to GMSL rise are estimated from observation-based
products.

Such processes include, but are not limited to, the impacts of diffusion, stirring, neutral physics, shortwave radiation, and
540 boundary fluxes, all of which alter oceanic density and thus affect GMSL. It is valuable to be able to close the GMSL rise
budget, as estimated from observations, by summing the contributions from the physical processes underlying changes in the
GMSL rise budget. This provides insight into the fundamental processes behind the observed global sea level rise and how
these processes may change in a transient ocean and climate.

This study provides a comparison of both the magnitude and uncertainty of the impact on GMSL by single processes or
545 parameterizations. With the observed GMSL rise currently being about 4 mm year^{-1} , this indicates that processes causing
changes of the order of 1 mm year^{-1} can be considered leading order terms in calculating GMSL rise. For accurately closing

the GMSL rise budget, one should arguably have an accuracy of about 0.1 mm year^{-1} . This immediately clarifies that it is not yet possible to close the GMSL budget using the bottom-up approach applied in this study.

For example, this study finds differences in GMSL rise estimates of about 30 and 40 mm year^{-1} between different boundary heat flux products or different mass flux products, respectively (Table 6). These estimates would improve if better observation-based constraints were available. Improving the mass and heatflux products is beyond the scope of this study. Instead, this study also used artificially balanced (i.e., globally net-zero) boundary mass and heat flux products for calculating the impacts on GMSL rise. Taken together, this study concludes that:

- It is currently not possible to close the GMSL rise budget using available ocean heat or mass flux products (sections 4.1, 4.3).
- Between different balanced heat flux products (no net global heating), differences in GMSL rise estimates are of the same order as the observed GMSL rise. This indicates that the spatial distribution of a heat flux product plays an important role for the GMSL rise budget (sections 4.1, 4.3).
- Mixing strength parameterizations have a leading-order impact on GMSL rise estimates (section 4.6).
- Implementation of neutral physics has a leading-order impact on GMSL rise estimates (section 4.8).
- The choice of shortwave radiation parameterizations has a leading-order impact on GMSL rise budgets, and its impact accumulates over time (Section 4.4).
- Parameterized eddy advection and freshwater fluxes have a second order impact on GMSL (sections 4.7 and 4.2).
- Nonlinear thermal expansion and densification upon mixing occur together, are of the same order of magnitude but of opposite sign, and therefore compensate each other. However, different time scales are involved for both processes due to differing physical mechanisms and geographical locations (Section 5).

The accuracy of the estimates is limited by both a lack of knowledge and observation-based constraints for several of the physical processes involved (e.g. boundary heat and mass fluxes, mixing, shortwave radiation), as well as due to the complexity to numerically implementing neutral physics. The above points should also be of interest to ocean modelers, as they must make specific choices about how to represent heat fluxes, mixing diffusivities, shortwave penetration, eddy stirring, and neutral physics. All these factors have a non-negligible impact on GMSL rise calculations. It remains unclear how the combination of these choices would impact GMSL rise predictions in, for example, IPCC-class models, as these require significant spin-up and equilibrium time during which some of these errors might balance out—or may lead to the right estimate for the wrong reason. It also raises the question if non-Boussinesq ocean models can accurately capture these impacts or will encounter too large uncertainties to obtain a realistic sea level budget from steric changes. Therefore, these results advocate for a thorough analysis of these processes in both models and observations, to improve understanding of such choices on GMSL rise predictions and increase the accuracy of predicted future sea level rise upon which policy will be based.

Code and data availability. World Ocean Atlas Garcia et al. (2019) data can be downloaded from <https://www.ncei.noaa.gov/data/oceans/woa/WOA18/DATA/>. TEOS-10 software McDougall and Barker (2011) can be downloaded from <https://www.teos-10.org/>. Observational estimates of the passive tracer diffusivity from Groeskamp et al. (2020) and related Matlab scripts are available at <https://doi.org/10.6084/m9.figshare.12554555.v2>. The climatological dissipation estimates of de Lavergne et al. (2020) are available at <https://www.seanoe.org/data/00619/73082/>. The VENM Matlab code of Groeskamp et al. (2019a) is available at <https://github.com/Sjoerdgr/VENM>. YoMaHa'07 Argo float trajectories based estimates at 1000 db (Lebedev et al., 2007) at <https://apdrc.soest.hawaii.edu/projects/yomaha/>. The Global Ocean Gridded L4 Sea Surface Heights data, provided by E.U. Copernicus Marine Service Information (CMEMS) can be found at Services (<https://doi.org/10.48670/moi-00148> (Accessed on 09-Dec-2024)). The OA flux (Yu et al., 2008) be found at <https://oafux.whoi.edu/data-access/>. CORE.v2 CORE2 Global Air-Sea Flux Dataset was downloaded from <http://rda.ucar.edu/datasets/ds260.2/>. The geothermal heatflux was downloaded from Goutorbe et al. (2011).

Appendix A: The material derivative of density

In Eq. 1, the material derivative of density is given by:

$$\frac{d\rho}{dt} = -\alpha\rho\frac{d\Theta}{dt} + \beta\rho\frac{dS_A}{dt} + \kappa\rho\frac{dP}{dt}. \quad (\text{A1})$$

Here $\frac{d\Theta}{dt}$, $\frac{dS_A}{dt}$ and $\frac{dP}{dt}$ are the material derivatives of Conservative Temperature Θ , Absolute Salinity S_A and pressure P , respectively. The thermal expansion coefficient α , the saline contraction coefficient β , and the isentropic compressibility κ are given by:

$$\alpha = -\frac{1}{\rho}\frac{\partial\rho}{\partial\Theta}|_{S_A,P}, \quad \beta = \frac{1}{\rho}\frac{\partial\rho}{\partial S_A}|_{\Theta,P}, \quad \kappa = \frac{1}{\rho}\frac{\partial\rho}{\partial P}|_{S_A,\Theta}. \quad (\text{A2})$$

Here the $|_{S_A,P}$ indicates that the derivative is obtained at constant S_A and P , etc. Changes in density are related to changes in S_A , Θ and P through α , β and κ . Because α , β and κ also depend on S_A , Θ and P , the equation of state is nonlinear. The convergence of heat and salt that can be written as:

$$\rho\frac{d\Theta}{dt} = -\nabla \cdot (\mathbf{J}_{\text{diff}}^{\Theta} + \mathbf{J}_{\text{stir}}^{\Theta}) + F_{\text{mass}}^{\Theta} + \rho F_{\text{source}}^{\Theta}, \quad (\text{A3})$$

$$\rho\frac{dS_A}{dt} = -\nabla \cdot (\mathbf{J}_{\text{diff}}^{S_A} + \mathbf{J}_{\text{stir}}^{S_A}) + F_{\text{mass}}^{S_A} + \rho F_{\text{source}}^{S_A}. \quad (\text{A4})$$

Here salt and heat changes due to convergence of diffusive fluxes are given by $\mathbf{J}_{\text{diff}}^{\Theta}$ and $\mathbf{J}_{\text{diff}}^{S_A}$ (in tracer $\text{kg m}^{-2} \text{s}^{-1}$), and include a diversity of mixing processes that are detailed in section 2.3. The minus sign assures positive numbers when heat or salt accumulate (converge). Salt and heat convergence due to advective subgridscale processes or 'skew fluxes' are given by $\mathbf{J}_{\text{stir}}^{\Theta}$ and $\mathbf{J}_{\text{stir}}^{S_A}$ (in tracer $\text{kg m}^{-2} \text{s}^{-1}$) (Gent and McWilliams, 1990; Gent et al., 1995; Griffies, 1998; McDougall and McIntosh, 2001). The changes of heat and salt due to boundary mass fluxes are given by F_{mass}^{Θ} and $F_{\text{mass}}^{S_A}$. Meanwhile the source terms $F_{\text{source}}^{S_A}$ and $F_{\text{source}}^{\Theta}$ (tracer $\text{kg m}^{-3} \text{s}^{-1}$) contain all other possible direct sources and sinks of salt and heat. Also the impact of pressure variations on density ($\kappa\frac{DP}{Dt}$, the last term in Eq. A1) is not accounted for. This is rationalized because 1) the impact is measurable but small (Dewar et al., 1998), and 2) Griffies and Greatbatch (2012) showed the impact on GMSL rise of this term is about 1000-10,000 times smaller than recent sea level rise estimates. As this term is difficult to calculate from observation-based products and almost negligible, it is not further investigated in this study.

610 Appendix B: Specifying the impact of boundary fluxes of salinity and temperature on density and sea level.

In this section the impact of mass and source fluxes of salinity and temperature are combined, to express their impact on density and sea level. Surface mass fluxes Q_{mass} change salinity and temperature through $F_{\text{mass}}^{S_A}$ and F_{mass}^{Θ} in Eq. A4. Combined, they alter density as follows:

$$F_{\text{mass}}^{\rho} = \underbrace{-\alpha Q_{\text{mass}} (\Theta_{\text{m}} - \Theta) \delta(z - \eta)}_{F_{\text{mass}}^{\Theta}} + \underbrace{\beta Q_{\text{mass}} (S_{\text{m}} - S_A) \delta(z - \eta)}_{F_{\text{mass}}^{S_A}}. \quad (\text{B1})$$

Here F_{mass}^{ρ} ($\text{kg m}^{-3} \text{ s}^{-1}$) contains Θ_{m} and S_{m} that are the mass-flux-weighted average of the salinity and temperature of the various components of the mass flux that are entering the ocean, while Θ and S_A are the oceanic values at the point of entry. The Dirac delta function $\delta(z - \eta)$ has units of inverse length (m^{-1}). Note that it is often assumed that the temperature of the mass flux equals the ocean such that $(\Theta_{\text{m}} - \Theta) = 0$, while the air-sea mass flux generally has a vanishing salinity ($S_{\text{m}} = 0$), making the salinity term an important term in the sea level budget (Nurser and Griffies, 2019).

Direct sources of salinity and heat at the surface of the ocean also impact the density budget. Surface heat fluxes ($F_{\text{surface}}^{\Theta}$, W m^{-2}) are given by longwave radiation as well as turbulent fluxes associated with latent and sensible heat. Surface salt fluxes (F_{surface}^S , $\text{g m}^{-2} \text{ s}^{-1}$) are associated with, but not limited to, sea ice or spray. This term can often be ignored, as is done in this study. The impact of these fluxes gives a change in density according to:

$$F_{\text{surface}}^{\rho} = \left(-\frac{\alpha}{C_p} F_{\text{surface}}^{\Theta} + \beta F_{\text{surface}}^S \right) \delta(z - \eta). \quad (\text{B2})$$

Here $F_{\text{surface}}^{\rho}$ is given in $\text{kg m}^{-3} \text{ s}^{-1}$ and C_p is the seawater heat capacity ($\text{J kg}^{-1} \text{ K}^{-1}$). At the ocean bottom, geothermal heating (F_{geo}^{Θ} , W m^{-2}) is a direct source of heat that alters the density budget as:

$$F_{\text{geo}}^{\rho} = -\frac{\alpha}{C_p} F_{\text{geo}}^{\Theta} \delta(z + H). \quad (\text{B3})$$

Here F_{geo}^{ρ} is given in $\text{kg m}^{-3} \text{ s}^{-1}$. Shortwave radiation (SWR) is a direct source of heat that enters the ocean at the surface and penetrates to deeper layers depending on the clarity of the water (Paulson and Simpson, 1977). The impact on density by convergence of SWR is given by:

$$F_{\text{swr}}^{\rho} = \left(\frac{\alpha}{C_p} \nabla \cdot \mathbf{J}_Q^{\text{swr}} \right) = \frac{\alpha}{C_p} Q_{\text{swr}} \frac{\partial F(z)}{\partial z}. \quad (\text{B4})$$

Here F_{swr}^{ρ} is given in $\text{kg m}^{-3} \text{ s}^{-1}$ and $\mathbf{J}_Q^{\text{swr}} = Q_{\text{swr}} F(z) \mathbf{k}$ is the amount of SWR at the surface (Q_{swr} , W m^{-2}) spread over depth according to the function $F(z)$. The convergence of this depth-dependent influx leads to a net heating (hence the extra minus sign to assure positive convergence). This study compares the following three realizations of $F(z)$:

$$F_{\text{SF}} = \begin{cases} 1 & \text{if } z = 0 \\ 0 & \text{if } z > 0 \end{cases} \quad (\text{B5})$$

$$F_{\text{PS77}} = R e^{-\frac{z}{h_1}} + (1 - R) e^{-\frac{z}{h_2}}, \quad (\text{B6})$$

$$F_{\text{MA94}} = I_{\text{IR}} + I_{\text{VIS}} \left(c_1 e^{-\frac{z}{\zeta_1}} + c_2 e^{-\frac{z}{\zeta_2}} \right), \quad (\text{B7})$$

For F_{SF} , all SWR is absorbed at the surface. F_{PS77} is an exponential decay function (Paulson and Simpson, 1977) in which $R = 0.58$, $h_1 = 0.35$ m, $h_2 = 23$ m, corresponding to Type-1 water from Jerlov (1968). In the equation for F_{MA94} , I_{IR} and I_{VIS} are the infrared and visible light components of the SWR, respectively (Morel and Antoine, 1994). All infrared radiation will be absorbed within 2 m (within the upper bin of the data used in this study), $I_{\text{IR}} = 0.43$ (Sweeney et al., 2005), where
635 $I_{\text{IR}} + I_{\text{VIS}} = 1$. The dependence of the depth penetration on Chlorophyll-a (Chl-a) for the visible component of the SWR, is included in the factors c_1 , c_2 , ζ_1 and ζ_2 in the exponents (which can be found in Table 2 of Morel and Antoine (1994)), such that $c_1 + c_2 = 1$, while ζ_1 and ζ_2 are e-folding depths (like h_1 and h_2).

Accounting for all considerations above, inserting that into Eq. 1 and using that $(\Theta_{\text{m}} - \Theta) = 0$, $S_{\text{m}} = 0$, $F_{\text{source}}^{S_A} = 0$ leaves:

$$\begin{aligned}
\left. \frac{\partial \eta}{\partial t} \right|_{\text{boundary}} &= - \int_H^\eta \frac{1}{\rho} (F_{\text{mass}}^\rho + F_{\text{surface}}^\rho + F_{\text{geo}}^\rho + F_{\text{swr}}^\rho) dz \\
640 \quad &= \left[\frac{\beta S_A}{\rho} Q_{\text{mass}} + \frac{\alpha}{\rho C_p} F_{\text{surface}}^\Theta \right]_\eta + \left[\frac{\alpha}{\rho C_p} F_{\text{geo}}^\Theta \right]_{-H} \\
&\quad - \int_H^\eta \frac{\alpha}{\rho C_p} Q_{\text{swr}} \frac{\partial f(z)}{\partial z} dz. \tag{B8}
\end{aligned}$$

Note that in this integral, even a net-zero global integral of the surface heat flux (including shortwave radiation), would lead to a non-zero integral due to a spatially varying factor $\alpha \rho^{-1}$, that for current planetary conditions leads to a net increase in sea level. Similar conceptual processes occur for the mass flux, salt flux and geothermal flux.

645 **Appendix C: Specifying the impact of diffusive fluxes of salinity and temperature on density and sea level.**

Here an expression is derived for the impact of diffusive mixing on density and sea level. Mixing is represented in a mixing tensor \mathbf{K} ($\text{m}^2 \text{s}^{-1}$) as a symmetric positive-definite kinematic diffusivity tensor that contains the contributions of the mesoscale neutral and horizontal diffusion, and small-scale isotropic diffusion (Fox-Kemper et al., 2019), which can be written as

$$\mathbf{K} = K_{\text{N}} (\mathbf{I} - \hat{\mathbf{n}}_\rho \hat{\mathbf{n}}_\rho) + K_{\text{H}} (\mathbf{I} - \mathbf{k} \mathbf{k}) + D \mathbf{I}. \tag{C1}$$

Here $\mathbf{k} = (0, 0, 1)$, \mathbf{I} is 3-dimensional the identity tensor. The dia-neutral unit vector $\hat{\mathbf{n}}_\rho = \nabla \rho_t / |\nabla \rho_t|^{-1}$ is defined according to
650 the gradient of locally referenced potential density ρ_t (McDougall et al., 2014), where $\nabla \rho_t = \rho(-\alpha \nabla \Theta + \beta \nabla S)$. The mixing tensor \mathbf{K} is written as:

$$\mathbf{K} \cdot \nabla \Theta = \underbrace{K_{\text{H}} \nabla_{\text{H}} \Theta}_{\text{horizontal}} + \underbrace{K_{\text{N}} \nabla_{\text{N}} \Theta}_{\text{neutral}} + \underbrace{D \frac{\partial \Theta}{\partial z} \mathbf{k}}_{\text{vertical}}, \tag{C2}$$

where $\nabla_{\text{N}} \Theta = (\mathbf{I} - \hat{\mathbf{n}}_\rho \hat{\mathbf{n}}_\rho) \cdot \nabla \Theta$, $\nabla_{\text{H}} \Theta = (\mathbf{I} - \mathbf{k} \mathbf{k}) \cdot \nabla \Theta$. It is used that it is a very good approximation if D only acts on vertical gradients. See McDougall et al. (2014) for a visual representation of the full and small-slope rotation tensor. A similar expression is obtained for salinity gradients, defined by the \mathbf{J}_{diff} -terms as the density weighted down-gradient diffusive tracer

655 concentration fluxes for S_A and Θ , given by:

$$\mathbf{J}_{\text{diff}}^{\Theta} = -\rho \mathbf{K} \cdot \nabla \Theta = \rho \mathbf{V}_{\Theta}, \quad \mathbf{J}_{\text{diff}}^{S_A} = -\rho \mathbf{K} \cdot \nabla S_A = \rho \mathbf{V}_{S_A}. \quad (\text{C3})$$

It helps to define $\mathbf{V}_{\Theta} = -\mathbf{K} \cdot \nabla \Theta$ and $\mathbf{V}_{S_A} = -\mathbf{K} \cdot \nabla S_A$ as the down-gradient diffusive tracer flux of Θ and S_A , respectively. The minus sign in the expression for the \mathbf{J}_{diff} -terms assures the down-gradient nature of the diffusive flux. The impact of mixing on sea level rise is obtained by inserting the \mathbf{J}_{diff} -terms into the last term on the r.h.s. of Eq. 1. This provides the component of sea level rise that is only due to diffusive fluxes of heat and salt that alter the density, and can be written as (Griffies and Greatbatch, 2012; Groeskamp et al., 2019b):

$$\left. \frac{\partial \eta}{\partial t} \right|_{\text{diffusion}} = - \int_{-H}^{\eta} \nu \left(\alpha \nabla \cdot \mathbf{J}_{\text{diff}}^{\Theta} - \beta \nabla \cdot \mathbf{J}_{\text{diff}}^{S_A} \right) dz. \quad (\text{C4})$$

Here $\nu = \rho^{-1}$ is specific volume ($\text{m}^3 \text{kg}^{-1}$). Using the following identities (Griffies and Greatbatch, 2012):

$$\nu \beta \nabla \cdot \rho \mathbf{V}_{S_A} = \nabla \cdot \beta \mathbf{V}_{S_A} - \mathbf{V}_{S_A} \cdot \nabla \beta - \beta \mathbf{V}_{S_A} \cdot \nabla \ln \rho, \quad (\text{C5})$$

$$\nu \alpha \nabla \cdot \rho \mathbf{V}_{\Theta} = \nabla \cdot \alpha \mathbf{V}_{\Theta} - \mathbf{V}_{\Theta} \cdot \nabla \alpha - \alpha \mathbf{V}_{\Theta} \cdot \nabla \ln \rho, \quad (\text{C6})$$

allows us to write

$$665 \quad \nu \alpha \nabla \cdot \mathbf{J}_{\text{diff}}^{\Theta} - \nu \beta \nabla \cdot \mathbf{J}_{\text{diff}}^{S_A} = \nabla \cdot \mathbf{R} - P - \mathbf{R} \cdot \nabla \ln \rho., \quad (\text{C7})$$

with:

$$\mathbf{R} = -\alpha \mathbf{K} \cdot \nabla \Theta + \beta \mathbf{K} \cdot \nabla S_A = \alpha \mathbf{V}_{\Theta} - \beta \mathbf{V}_{S_A} = \mathbf{R}^{\text{ntr}} + \mathbf{R}^{\text{hor}} + \mathbf{R}^{\text{ver}}, \quad (\text{C8})$$

$$P = \nabla \alpha \cdot (\mathbf{K} \cdot \nabla \Theta) - \nabla \beta \cdot (\mathbf{K} \cdot \nabla S_A) = \nabla \alpha \cdot \mathbf{V}_{\Theta} - \nabla \beta \cdot \mathbf{V}_{S_A}, \quad (\text{C9})$$

$$= P^{\text{ntr}} + P^{\text{hor}} + P^{\text{ver}}.$$

Here \mathbf{R}^{ntr} , \mathbf{R}^{hor} , and \mathbf{R}^{ver} (m s^{-1}) are the components of \mathbf{R} for the three different mixing direction, while P^{ntr} , P^{hor} , and P^{ver} are the components of P (s^{-1}) for the three different mixing direction. The full expressions for \mathbf{R}^{ntr} , \mathbf{R}^{hor} , and \mathbf{R}^{ver} are given by

$$670 \quad \mathbf{R}^{\text{ntr}} = -K_N [\alpha \nabla_N \Theta - \beta \nabla_N S_A] = 0,$$

$$\mathbf{R}^{\text{hor}} = -K_H [\alpha \nabla_H \Theta - \beta \nabla_H S_A],$$

$$\mathbf{R}^{\text{ver}} = -D \left[-\alpha \frac{\partial \Theta}{\partial z} + \beta \frac{\partial S_A}{\partial z} \right] \mathbf{k}. \quad (\text{C10})$$

By definition, for the neutral direction $\alpha \nabla_N \Theta = \beta \nabla_N S_A$ and therefore $\mathbf{R}^{\text{ntr}} = 0$. The full expressions for P^{ntr} , P^{hor} , and P^{ver} are given by

$$675 \quad P^{\text{ntr}} = K_N (\nabla_N \alpha \cdot \nabla_N \Theta - \nabla_N \beta \cdot \nabla_N S_A) = P_{T_b}^{\text{ntr}} + P_{C_b}^{\text{ntr}},$$

$$P^{\text{hor}} = K_H (\nabla_H \alpha \cdot \nabla_H \Theta - \nabla_H \beta \cdot \nabla_H S_A) = P_{T_b}^{\text{hor}} + P_{C_b}^{\text{hor}},$$

$$P^{\text{ver}} = D \left(\frac{\partial \alpha}{\partial z} \frac{\partial \Theta}{\partial z} - \frac{\partial \beta}{\partial z} \frac{\partial S_A}{\partial z} \right) = P_{T_b}^{\text{ver}} + P_{C_b}^{\text{ver}}. \quad (\text{C11})$$

Where the production terms in Eq. C11 are further expanded into the more well know cabbeling and thermobaricity components, for which the expressions are provided in Eq. C17 to Eq. C22 in Appendix C1. When inserting Eq. (C7) into Eq. (C4) and applying the Leibniz integral rule for differentiation under an integral to rewrite the $\nabla \cdot \mathbf{R}$ term (see Appendix C2), to obtain

$$\begin{aligned} \left. \frac{\partial \eta}{\partial t} \right|_{\text{diffusion}} &= -\nabla_{\mathbf{H}} \cdot \int_{-H}^{\eta} \mathbf{R} dz + \mathbf{R}(\eta) \cdot \nabla_{\mathbf{H}} \eta - \mathbf{R}(-H) \cdot \nabla_{\mathbf{H}}(-H) \\ &+ \int_{-H}^{\eta} P dz + \int_{-H}^{\eta} \mathbf{R} \cdot \nabla \ln(\rho) dz. \end{aligned} \quad (\text{C12})$$

As there are no diffusive fluxes through any of the ocean boundaries, a global integral of $\left. \frac{\partial \eta}{\partial t} \right|_{\text{diffusion}}$ would cause the first term on the r.h.s. to vanish. Hence, comparable to volume redistribution by ocean currents, this term locally changes sea level without a net global effect. Even though this only applies to the first term on the r.h.s. of Eq. C12 where \mathbf{R} is involved, this inspired the naming of " \mathbf{R} " as "redistribution" term. All other terms in the equation, have both a local and net global contribution to GMSL. Of special interest is the term P, that is directly related to cabbeling and thermobaricity in all three mixing direction (McDougall, 1987b), as detailed in Appendix C1. To further develop the impact of ocean mixing on sea level rise, the following steps are applied. First 1) use that there are no fluxes through the boundaries, thus $\mathbf{R}^{\text{ver}}(H) = \mathbf{R}^{\text{ver}}(\eta) = 0$, and the vertical integral of $\partial \mathbf{R}^{\text{ver}} / \partial z$ is zero, 2) write $P = P_{\text{T}_b}^{\text{ntr}} + P_{\text{C}_b}^{\text{ntr}} + P_{\text{C}_b}^{\text{hor}} + P_{\text{T}_b}^{\text{hor}} + P_{\text{T}_b}^{\text{ver}} + P_{\text{C}_b}^{\text{ver}}$, and 3) rewrite $\nabla \ln \rho \cdot \mathbf{R}$ using the identity $\nabla \ln(\rho) \cdot \mathbf{R} = \nu \mathbf{R} \cdot \nabla \rho$ in combination with the specific mixing direction to write these terms from Eq. C12 as:

$$\nabla_{\mathbf{H}} \ln(\rho) \cdot \mathbf{R}^{\text{hor}} = K_{\mathbf{H}}^{-1} |\mathbf{R}^{\text{hor}}|^2 + \kappa \nabla_{\mathbf{H}} P \cdot \mathbf{R}^{\text{hor}} \approx K_{\mathbf{H}}^{-1} |\mathbf{R}^{\text{hor}}|^2 \quad (\text{C13})$$

$$\frac{\partial \ln(\rho)}{\partial z} \mathbf{k} \cdot \mathbf{R}^{\text{ver}} = D^{-1} |\mathbf{R}^{\text{ver}}|^2 - \rho g \kappa \mathbf{k} \cdot \mathbf{R}^{\text{ver}} \quad (\text{C14})$$

$$\nabla_{\mathbf{N}} \ln(\rho) \cdot \mathbf{R}^{\text{ntr}} = K_{\mathbf{N}}^{-1} |\mathbf{R}^{\text{ntr}}|^2 + \kappa \nabla_{\mathbf{N}} P \cdot \mathbf{R}^{\text{ntr}} \quad (\text{C15})$$

Inserting this all these points into Eq. C12, leaves the final expression for the impact of diffusive fluxes on sea level:

$$\begin{aligned} \left. \frac{\partial \eta}{\partial t} \right|_{\text{diffusion}} &\approx -\nabla_{\mathbf{H}} \cdot \underbrace{\int_{-H}^{\eta} \mathbf{R}^{\text{hor}} dz}_{\text{Redistribution}} + \mathbf{R}^{\text{hor}}(\eta) \cdot \nabla_{\mathbf{H}} \eta - \mathbf{R}^{\text{hor}}(-H) \cdot \nabla_{\mathbf{H}}(-H) \\ &+ \int_{-H}^{\eta} K_{\mathbf{H}}^{-1} |\mathbf{R}^{\text{hor}}|^2 dz + \int_{-H}^{\eta} D^{-1} |\mathbf{R}^{\text{ver}}|^2 dz - \int_{-H}^{\eta} \rho g \kappa \mathbf{k} \cdot \mathbf{R}^{\text{ver}} dz \\ &+ \int_{-H}^{\eta} P_{\text{T}_b}^{\text{ntr}} + P_{\text{C}_b}^{\text{ntr}} + P_{\text{C}_b}^{\text{hor}} + P_{\text{T}_b}^{\text{ver}} + P_{\text{C}_b}^{\text{ver}} dz. \end{aligned} \quad (\text{C16})$$

700 C1 The Production terms expanded

The production term of Eq. (C10) can be rewritten using the mixing tensor of Eq. (C2) into the more well know cabbeling and thermobaricity components. The expression below allow us to see the similarities between thermobaricity and cabbeling

(densification upon mixing) for the different mixing direction:

$$P_{T_b}^{\text{ntnr}} = K_N T_b \nabla_N P \cdot \nabla_N \Theta, \quad (\text{C17})$$

$$705 \quad P_{C_b}^{\text{ntnr}} = K_N C_b |\nabla_N \Theta|^2, \quad (\text{C18})$$

$$P_{T_b}^{\text{hor}} = K_H \nabla_H P \cdot \left(\frac{\partial \alpha}{\partial p} \nabla_H \Theta - \frac{\partial \beta}{\partial p} \nabla_H S_A \right) \\ = K_H T_b^{\text{hor}} \nabla_H P \cdot \nabla_H \Theta \quad (\text{C19})$$

$$P_{C_b}^{\text{hor}} = K_H \left(\frac{\partial \alpha}{\partial \Theta} |\nabla_H \Theta|^2 + 2 \frac{\partial \alpha}{\partial S_A} \nabla_H S_A \cdot \nabla_H \Theta - \frac{\partial \beta}{\partial S_A} |\nabla_H S_A|^2 \right) \\ = K_H C_b^{\text{hor}} |\nabla_H \Theta|^2 \quad (\text{C20})$$

$$710 \quad P_{T_b}^{\text{ver}} = -D \rho g \left(\frac{\partial \alpha}{\partial P} \frac{\partial \Theta}{\partial z} - \frac{\partial \beta}{\partial P} \frac{\partial S_A}{\partial z} \right) \\ = -D \rho g T_b^{\text{ver}} \frac{\partial \Theta}{\partial z} \quad (\text{C21})$$

$$P_{C_b}^{\text{ver}} = D \left(\frac{\partial \alpha}{\partial \Theta} \left| \frac{\partial \Theta}{\partial z} \right|^2 + 2 \frac{\partial \alpha}{\partial S_A} \frac{\partial S_A}{\partial z} \frac{\partial \Theta}{\partial z} - \frac{\partial \beta}{\partial S_A} \left| \frac{\partial S_A}{\partial z} \right|^2 \right) \\ = D C_b^{\text{ver}} \left| \frac{\partial \Theta}{\partial z} \right|^2 \quad (\text{C22})$$

In order to break down Eq. C11 into Eqs. (C17) - (C22), we use variables and identities define below. First, C_b (K^{-2}) and T_b ($\text{Pa}^{-1} \text{K}^{-1}$) are the cabbeling and thermobaricity coefficients for the neutral direction, as previously defined by (McDougall, 1984, 1987a) given by

$$C_b = \frac{\partial \alpha}{\partial \Theta} + 2 \frac{\alpha}{\beta} \frac{\partial \alpha}{\partial S_A} - \frac{\alpha^2}{\beta^2} \frac{\partial \beta}{\partial S_A}, \quad T_b = \frac{\partial \alpha}{\partial P} - \frac{\alpha}{\beta} \frac{\partial \beta}{\partial P}. \quad (\text{C23})$$

This study introduces C_b^{ver} and C_b^{hor} (K^{-2}) and T_b^{ver} and T_b^{hor} ($\text{Pa}^{-1} \text{K}^{-1}$) as the vertical and horizontal equivalents of their neutral counterparts, given by:

$$720 \quad C_b^{\text{hor}} = \frac{\partial \alpha}{\partial \Theta} + 2 \frac{\alpha}{\beta} \frac{\partial \alpha}{\partial S_A} \frac{1}{R_H} - \frac{\alpha^2}{\beta^2} \frac{\partial \beta}{\partial S_A} \frac{1}{R_H^2}, \quad T_b^{\text{hor}} = \frac{\partial \alpha}{\partial P} - \frac{\alpha}{\beta} \frac{\partial \beta}{\partial P} \frac{1}{R_H}, \quad (\text{C24})$$

$$C_b^{\text{ver}} = \frac{\partial \alpha}{\partial \Theta} + 2 \frac{\alpha}{\beta} \frac{\partial \alpha}{\partial S_A} \frac{1}{R_\rho} - \frac{\alpha^2}{\beta^2} \frac{\partial \beta}{\partial S_A} \frac{1}{R_\rho^2}, \quad T_b^{\text{ver}} = \frac{\partial \alpha}{\partial P} - \frac{\alpha}{\beta} \frac{\partial \beta}{\partial P} \frac{1}{R_\rho}. \quad (\text{C25})$$

Here

$$R_\rho = \frac{\alpha}{\beta} \frac{\frac{\partial \Theta}{\partial z}}{\frac{\partial S_A}{\partial z}}, \quad \text{and} \quad R_H = \frac{\alpha}{\beta} \frac{\nabla_H \Theta}{\nabla_H S_A} \quad (\text{C26})$$

are the vertical R_ρ and horizontal stability ratio R_H . Although the latter may have less physical meaning in turbulence theory, it is of symbolic use for comparing between the newly defined horizontal and vertical cabbeling and thermobaricity terms. To obtain Eq. (C23-C25), use that ρ , α , β and κ are given by polynomials, such that Clairaut's theorem can be used:

$$\frac{\partial}{\partial \varphi} \frac{1}{\rho} \frac{\partial \rho}{\partial \phi} = \frac{1}{\rho} \frac{\partial^2 \rho}{\partial \varphi \partial \phi} + \frac{1}{\rho^2} \frac{\partial \rho}{\partial \phi} \frac{\partial \rho}{\partial \varphi} = \frac{1}{\rho} \frac{\partial^2 \rho}{\partial \phi \partial \varphi} + \frac{1}{\rho^2} \frac{\partial \rho}{\partial \varphi} \frac{\partial \rho}{\partial \phi} = \frac{\partial}{\partial \phi} \frac{1}{\rho} \frac{\partial \rho}{\partial \varphi}. \quad (\text{C27})$$

This is used to fill in the nine different combination (using S_A , Θ or P) and obtain the following identities (McDougall, 1984, 1987a):

$$730 \quad -\frac{\partial \alpha}{\partial S_A} = \frac{\partial \beta}{\partial \Theta}, \quad -\frac{\partial \alpha}{\partial P} = \frac{\partial \kappa}{\partial \Theta}, \quad \frac{\partial \beta}{\partial P} = \frac{\partial \kappa}{\partial S_A}. \quad (\text{C28})$$

In addition, this study uses that:

$$\nabla \alpha = \frac{\partial \alpha}{\partial \Theta} \nabla \Theta + \frac{\partial \alpha}{\partial S_A} \nabla S_A + \frac{\partial \alpha}{\partial p} \nabla P, \quad (\text{C29})$$

$$\nabla \beta = \frac{\partial \beta}{\partial \Theta} \nabla \Theta + \frac{\partial \beta}{\partial S_A} \nabla S_A + \frac{\partial \beta}{\partial p} \nabla P, \quad (\text{C30})$$

C2 Leibniz Rule applied to \mathbf{R}

735 To obtain Eq.(C12) from Eq. (C4) the Leibniz integral rule for differentiation under an integral is used:

$$\frac{\partial}{\partial x} \int_{a(x)}^{b(x)} f(x,t) dt = \int_{a(x)}^{b(x)} \frac{\partial f(x,t)}{\partial x} dt + f(x,b(x)) \frac{\partial b(x)}{\partial x} - f(x,a(x)) \frac{\partial a(x)}{\partial x}. \quad (\text{C31})$$

This can also be written as:

$$\int_{a(x)}^{b(x)} \frac{\partial f(x,t)}{\partial x} dt = \frac{\partial}{\partial x} \int_{a(x)}^{b(x)} f(x,t) dt - f(x,b(x)) \frac{\partial b(x)}{\partial x} + f(x,a(x)) \frac{\partial a(x)}{\partial x}. \quad (\text{C32})$$

Using $\mathbf{R} = (R_x, R_y, R_z)$, this allows us to write:

$$740 \quad \int_{-H}^{\eta} \frac{\partial R_x}{\partial x} dz = \frac{\partial}{\partial x} \int_{-H}^{\eta} R_x dz - R_x(\eta) \frac{\partial \eta}{\partial x} + R_x(-H) \frac{\partial(-H)}{\partial x}, \quad (\text{C33})$$

$$\int_{-H}^{\eta} \frac{\partial R_y}{\partial y} dz = \frac{\partial}{\partial y} \int_{-H}^{\eta} R_y dz - R_y(\eta) \frac{\partial \eta}{\partial y} + R_y(-H) \frac{\partial(-H)}{\partial y}, \quad (\text{C34})$$

$$\int_{-H}^{\eta} \frac{\partial R_z}{\partial z} dz = R_z(\eta) - R_z(-H) = 0 \quad (\text{No diffusion through boundary}). \quad (\text{C35})$$

Which leaves:

$$\int_{-H}^{\eta} \nabla \cdot \mathbf{R} dz = \nabla_H \cdot \int_{-H}^{\eta} \mathbf{R} dz - \mathbf{R}(\eta) \cdot \nabla_H \eta + \mathbf{R}(-H) \cdot \nabla_H(-H). \quad (\text{C36})$$

745 Appendix D: Specifying the sea level change due to eddy-induced transport

Here the impact of quasi-Stokes transport on sea level is derived. First the eddy-induced velocity (u^*, v^*, w^*) is defined using the eddy induced transport Υ as:

$$\mathbf{u}_{\text{eddy}} = (u^*, v^*, w^*) = \left(\frac{\partial \Upsilon}{\partial z}, -\nabla \cdot \Upsilon \right). \quad (\text{D1})$$

Ferrari et al. (2010) argued that the eddy induced transport should be zero at the ocean surface and bottom $\Upsilon(\eta) = \Upsilon(-H) = 0$,
 750 to ensure a zero barotropic component due to the eddy-induced velocity. The vertical integral of the eddy-induced velocity,
 which is a component of \mathbf{u} in Eq. 1, is then zero. Yet, the eddy-induced transport will impact density by transporting salt and
 heat. Following Griffies (1998), this impact can be written as a density weighted skew flux given by:

$$\mathbf{J}_{\text{stir}}^{\Theta} = -\rho \mathbf{K}_{\text{stir}} \cdot \nabla \Theta = \rho \mathbf{V}_{\text{stir}}^{\Theta}, \quad \mathbf{J}_{\text{stir}}^{S_A} = -\rho \mathbf{K}_{\text{stir}} \cdot \nabla S_A = \rho \mathbf{V}_{\text{stir}}^{S_A}. \quad (\text{D2})$$

Where:

$$\mathbf{K}_{\text{stir}} = \begin{pmatrix} 0 & 0 & \Upsilon^{(x)} \\ 0 & 0 & \Upsilon^{(y)} \\ -\Upsilon^{(x)} & -\Upsilon^{(y)} & 0 \end{pmatrix}, \quad (\text{D3})$$

755 and

$$\mathbf{V}_{\text{stir}}^{\Theta} = -\mathbf{K}_{\text{stir}} \cdot \nabla \Theta = \left(\Upsilon^x \frac{\partial \Theta}{\partial z}, \Upsilon^y \frac{\partial \Theta}{\partial z}, -\Upsilon \cdot \nabla_H \Theta \right), \quad (\text{D4})$$

$$\mathbf{V}_{\text{stir}}^{S_A} = -\mathbf{K}_{\text{stir}} \cdot \nabla S_A = \left(\Upsilon^x \frac{\partial S_A}{\partial z}, \Upsilon^y \frac{\partial S_A}{\partial z}, -\Upsilon \cdot \nabla_H S_A \right). \quad (\text{D5})$$

Hence $\mathbf{V}_{\text{stir}}^{\Theta}$ and $\mathbf{V}_{\text{stir}}^{S_A}$ are the down gradient eddy tracer flux of temperature and salinity, respectively. Following Gent et al.
 (1995); McDougall and McIntosh (2001); Ferrari et al. (2010) the eddy transport flux ($\text{m}^2 \text{s}^{-1}$) is defined as:

$$\Upsilon^x = -K_{\text{stir}} S_x f_{\text{stir}}(z), \quad \Upsilon^y = -K_{\text{stir}} S_y f_{\text{stir}}(z). \quad (\text{D6})$$

Here K_{stir} is the stirring strength, also known as the GM diffusivity (Gent and McWilliams, 1990), S_x and S_y are neutral
 760 slopes and $f_{\text{stir}}(z)$ is some vertical tapering function that assures that $\Upsilon = (\Upsilon^x, \Upsilon^y)$ satisfies the boundary condition $\Upsilon(\eta) =$
 $\Upsilon(-H) = 0$. For the vertical tapering function $f_{\text{stir}}(z)$ a linear tapering between 0 and 1 is used over the upper 400 m from
 the surface down and from the bottom up. Analogous to Eq. C7 it is found that:

$$\nu \alpha \nabla \cdot \mathbf{J}_{\text{stir}}^{\Theta} - \nu \beta \nabla \cdot \mathbf{J}_{\text{stir}}^{S_A} = \nabla \cdot \mathbf{R}_{\text{stir}} - P_{\text{stir}} - \mathbf{R}_{\text{stir}} \cdot \nabla \ln \rho. \quad (\text{D7})$$

With:

$$\begin{aligned} \mathbf{R}_{\text{stir}} &= \alpha \mathbf{V}_{\text{stir}}^{\Theta} - \beta \mathbf{V}_{\text{stir}}^{S_A}, \\ &= \Upsilon^x \left[\alpha \frac{\partial \Theta}{\partial z} - \beta \frac{\partial S_A}{\partial z} \right] \mathbf{i} + \Upsilon^y \left[\alpha \frac{\partial \Theta}{\partial z} - \beta \frac{\partial S_A}{\partial z} \right] \mathbf{j} \\ &\quad - \Upsilon^x \left[\alpha \frac{\partial \Theta}{\partial x} - \beta \frac{\partial S_A}{\partial x} \right] \mathbf{k} - \Upsilon^y \left[\alpha \frac{\partial \Theta}{\partial y} - \beta \frac{\partial S_A}{\partial y} \right] \mathbf{k}, \end{aligned} \quad (\text{D8})$$

$$\begin{aligned} P_{\text{stir}} &= \nabla \alpha \cdot \mathbf{V}_{\text{stir}}^{\Theta} - \nabla \beta \cdot \mathbf{V}_{\text{stir}}^{S_A} \\ &= \Upsilon^x \left(\frac{\partial \Theta}{\partial z} \frac{\partial \alpha}{\partial x} - \frac{\partial \Theta}{\partial x} \frac{\partial \alpha}{\partial z} - \frac{\partial S_A}{\partial z} \frac{\partial \beta}{\partial x} + \frac{\partial S_A}{\partial x} \frac{\partial \beta}{\partial z} \right) \\ &\quad + \Upsilon^y \left(\frac{\partial \Theta}{\partial z} \frac{\partial \alpha}{\partial y} - \frac{\partial \Theta}{\partial y} \frac{\partial \alpha}{\partial z} - \frac{\partial S_A}{\partial z} \frac{\partial \beta}{\partial y} + \frac{\partial S_A}{\partial y} \frac{\partial \beta}{\partial z} \right). \end{aligned} \quad (\text{D9})$$

765 Inserting Eq. D7 into Eq. 1, and using the Leibniz rule again, gives the impact of stirring on sea level evolution given by:

$$\begin{aligned}
\left. \frac{\partial \eta}{\partial t} \right|_{\text{stirring}} &= - \int_{-H}^{\eta} \nu \left(\alpha \nabla \cdot \mathbf{J}_{\text{stir}}^{\Theta} - \beta \nabla \cdot \mathbf{J}_{\text{stir}}^{S_A} \right) dz, \\
&= - \nabla_H \cdot \int_{-H}^{\eta} \mathbf{R}_{\text{stir}} dz + \int_{-H}^{\eta} P_{\text{stir}} dz + \int_{-H}^{\eta} \mathbf{R}_{\text{stir}} \cdot \nabla \ln \rho dz.
\end{aligned} \tag{D10}$$

Here it is used that the boundaries $\Upsilon = 0$ and that the vertical integral of \mathbf{R}_{stir} is zero. Now using the same identity as for Eq. C13 - Eq. C15, for computer coding purposes, the last term on the r.h.s. is expanded as:

$$\begin{aligned}
770 \int_{-H}^{\eta} \mathbf{R}_{\text{stir}} \cdot \nabla \ln \rho dz &= \int_{-H}^{\eta} \nu \mathbf{R}_{\text{stir}} \cdot \nabla \rho dz, \\
&= \int_{-H}^{\eta} \mathbf{R}_{\text{stir}} \cdot \left(-\alpha \nabla \Theta + \beta \nabla S_A + \kappa \nabla P \right) dz, \\
&= \int_{-H}^{\eta} \Upsilon^x \left[\alpha \frac{\partial \Theta}{\partial z} - \beta \frac{\partial S_A}{\partial z} \right] \left(-\alpha \frac{\partial \Theta}{\partial x} + \beta \frac{\partial S_A}{\partial x} + \kappa \frac{\partial P}{\partial x} \right) dz, \\
&+ \int_{-H}^{\eta} \Upsilon^y \left[\alpha \frac{\partial \Theta}{\partial z} - \beta \frac{\partial S_A}{\partial z} \right] \left(-\alpha \frac{\partial \Theta}{\partial y} + \beta \frac{\partial S_A}{\partial y} + \kappa \frac{\partial P}{\partial y} \right) dz, \\
&+ \int_{-H}^{\eta} - \left(\Upsilon^x \left[\alpha \frac{\partial \Theta}{\partial x} - \beta \frac{\partial S_A}{\partial x} \right] + \Upsilon^y \left[\alpha \frac{\partial \Theta}{\partial y} - \beta \frac{\partial S_A}{\partial y} \right] \right) \left(-\alpha \frac{\partial \Theta}{\partial z} + \beta \frac{\partial S_A}{\partial z} - \kappa \rho g \right) dz.
\end{aligned} \tag{D11}$$

775

Through Eq. D6, stirring depends on the accuracy of the calculated neutral slope. This allows us to define the impact of non-neutrality on stirring and sea level as:

$$\begin{aligned}
\Upsilon_{\text{non-neutral}}^x &= -K_{\text{stir}} (S_x - S_x^{\text{(perfectly neutral)}}) f_{\text{stir}}(z), \\
\Upsilon_{\text{non-neutral}}^y &= -K_{\text{stir}} (S_y - S_y^{\text{(perfectly neutral)}}) f_{\text{stir}}(z).
\end{aligned} \tag{D12}$$

780 An overestimate of the neutral slopes will lead to more reduction in GMSL by eddy stirring.

Appendix E: Balancing the heat fluxes

To construct the balanced heat and mass fluxes, this study distributes the global mass or heat imbalance over all grid points and time, proportionally to the local flux. Larger flux terms compensate for a larger fraction of the imbalance for a grid point. Here the mass flux is used to illustrate the procedure, but the same procedure is applied to the heat fluxes. First, define the

785 global mass imbalances as ϵ (kg s^{-1}), which is determined for the different mass flux components (note that the contribution

for evaporation E are split in a positive and negative part):

$$\epsilon_P = \int_{\text{global}} P dA, \quad \epsilon_R = \int_{\text{global}} R dA, \quad \epsilon_{E>0} = \int_{\text{global}} (E > 0) dA, \quad \text{and} \quad \epsilon_{E<0} = \int_{\text{global}} (E < 0) dA. \quad (\text{E1})$$

Then the total net flux imbalance ϵ_q is calculated, as well as the total flux exchange that has occurred $\epsilon_{|q|}$. This is the sum of the absolute values:

$$\epsilon_q = \epsilon_P + \epsilon_R + \epsilon_{E<0} + \epsilon_{E>0}, \quad (\text{E2})$$

$$\epsilon_{|q|} = |\epsilon_P| + |\epsilon_R| + |\epsilon_{E<0}| + |\epsilon_{E>0}| + |\epsilon_{E>0}|. \quad (\text{E3})$$

Note that ϵ_q is equal to $\int_{\text{global}} Q_m dA$ and thus the total global net mass flux. Now define a vector of the individual flux terms
790 and exchange terms:

$$\mathbf{L} = [\epsilon_P, \epsilon_R, \epsilon_{E<0}, \epsilon_{E>0}], \quad (\text{E4})$$

$$\mathbf{L}_A = [|\epsilon_P|, |\epsilon_R|, |\epsilon_{E<0}|, |\epsilon_{E>0}|]. \quad (\text{E5})$$

The above definitions are used to redistribute the imbalance over all the terms. Then compute the fraction r that each term should compensate for, with respect to the total exchange with the ocean:

$$r = \epsilon_{|q|}^{-1} \mathbf{L}_A \quad (\text{E6})$$

The sum of r is 1, and each number is the fraction that a mass flux term needs to compensate in total. Using this, the new imbalances are defined (e.g. ϵ_P^0 instead of ϵ_P) that are the new globally integrated total fluxes for each individual term, such
795 that the net global imbalance adds up to zero:

$$[\epsilon_P^0, \epsilon_R^0, \epsilon_{E<0}^0, \epsilon_{E>0}^0] = \mathbf{L} - r \epsilon_q = \mathbf{L} - \frac{\epsilon_q}{\epsilon_{|q|}} \mathbf{L}_A \quad (\text{E7})$$

The new "balanced" mass flux then becomes:

$$P_b(x, y, t) = P(x, y, t) \frac{\epsilon_P^0}{\epsilon_P} \quad (\text{E8})$$

$$R_b(x, y, t) = R(x, y, t) \frac{\epsilon_R^0}{\epsilon_R} \quad (\text{E9})$$

$$(E > 0)_b(x, y, t) = (E > 0)(x, y, t) \frac{\epsilon_{E>0}^0}{\epsilon_{E>0}} \quad (\text{E10})$$

$$(E < 0)_b(x, y, t) = (E < 0)(x, y, t) \frac{\epsilon_{E<0}^0}{\epsilon_{E<0}} \quad (\text{E11})$$

$$E_b(x, y, t) = (E > 0)_b(x, y, t) + (E < 0)_b(x, y, t) \quad (\text{E12})$$

A similar exercise is done with the heat fluxes.

Author contributions. Sjoerd Groeskamp is the sole author.

Competing interests. The author is a member of the editorial board of Ocean Science (OS)

800 *Acknowledgements.* I thank Stephen Griffies for useful comments on an early draft of this work, Anja Mödl for doing some early calculations on this work with me, as part of her MSc thesis. I thank Ryan Abernathey, Magnus Hieronymus for discussions on the nonlinear equation of state. I thank Aimee Slangen for useful discussion on this topic. I thank 2 anonymous reviewers for their very detailed reviews that helped to improve the paper a lot.

References

- 805 Abernathy, R., Ferreira, D., and Klocker, A.: Diagnostics of isopycnal mixing in a circumpolar channel, *Ocean Modelling*, 72, 1–16, <https://doi.org/http://dx.doi.org/10.1016/j.ocemod.2013.07.004>, 2013.
- Abernathy, R. P. and Marshall, J.: Global surface eddy diffusivities derived from satellite altimetry, *Journal of Geophysical Research: Oceans*, 118, 901–916, <https://doi.org/10.1002/jgrc.20066>, 2013.
- Ablain, M., Legeais, J. F., Prandi, P., Marcos, M., Fenoglio-Marc, L., Dieng, H. B., Benveniste, J., and Cazenave, A.: Satellite Altimetry-
810 Based Sea Level at Global and Regional Scales, *Surveys in Geophysics*, 38, 7–31, <https://doi.org/10.1007/s10712-016-9389-8>, 2017.
- Adcroft, A., Anderson, W., Balaji, V., Blanton, C., Bushuk, M., Dufour, C. O., Dunne, J. P., Griffies, S. M., Hallberg, R., Harrison, M. J., Held, I. M., Jansen, M. F., John, J. G., Krasting, J. P., Langenhorst, A. R., Legg, S., Liang, Z., McHugh, C., Radhakrishnan, A., Reichl, B. G., Rosati, T., Samuels, B. L., Shao, A., Stouffer, R., Winton, M., Wittenberg, A. T., Xiang, B., Zadeh, N., and Zhang, R.: The GFDL Global Ocean and Sea Ice Model OM4.0: Model Description and Simulation Features, *Journal of Advances in Modeling Earth Systems*,
815 11, 3167–3211, <https://doi.org/10.1029/2019MS001726>, 2019.
- Adler, R. F., Huffman, G. J., Chang, A., Ferraro, R., Xie, P.-P., Janowiak, J., Rudolf, B., Schneider, U., Curtis, S., Bolvin, D., Gruber, A., Susskind, J., Arkin, P., and Nelkin, E.: The Version-2 Global Precipitation Climatology Project (GPCP) Monthly Precipitation Analysis (1979–Present), *Journal of Hydrometeorology*, 4, 1147–1167, [https://doi.org/10.1175/1525-7541\(2003\)004<1147:TVGPCP>2.0.CO;2](https://doi.org/10.1175/1525-7541(2003)004<1147:TVGPCP>2.0.CO;2), 2003.
- 820 Antonov, J. I., Levitus, S., and Boyer, T. P.: Steric sea level variations during 1957–1994: Importance of salinity, *Journal of Geophysical Research: Oceans*, 107, SRF 14–1–SRF 14–8, <https://doi.org/https://doi.org/10.1029/2001JC000964>, 2002.
- Balmaseda, M. A., Hernandez, F., Storto, A., Palmer, M. D., Alves, O., Shi, L., Smith, G. C., Toyoda, T., Valdivieso, M., Barnier, B., Behringer, D., Boyer, T., Chang, Y.-S., Chepurin, G. A., Ferry, N., Forget, G., Fujii, Y., Good, S., Guinehut, S., Haines, K., Ishikawa, Y., Keeley, S., Köhl, A., Lee, T., Martin, M. J., Masina, S., Masuda, S., Meyssignac, B., Mogensen, K., Parent, L., Peterson, K. A., Tang,
825 Y. M., Yin, Y., Vernieres, G., Wang, X., Waters, J., Wedd, R., Wang, O., Xue, Y., Chevallier, M., Lemieux, J.-F., Dupont, F., Kuragano, T., Kamachi, M., Awaji, T., Caltabiano, A., Wilmer-Becker, K., and Gaillard, F.: The Ocean Reanalyses Intercomparison Project (ORA-IP), *Journal of Operational Oceanography*, 8, s80–s97, <https://doi.org/10.1080/1755876X.2015.1022329>, 2015.
- Barker, P. M. and McDougall, T. J.: Two Interpolation Methods Using Multiply-Rotated Piecewise Cubic Hermite Interpolating Polynomials, *Journal of Atmospheric and Oceanic Technology*, 37, 605–619, <https://doi.org/10.1175/JTECH-D-19-0211.1>, 2020.
- 830 Church, J. A., White, N. J., Konikow, L. F., Domingues, C. M., Cogley, J. G., Rignot, E., Gregory, J. M., van den Broeke, M. R., Monaghan, A. J., and Velicogna, I.: Revisiting the Earth’s sea-level and energy budgets from 1961 to 2008, *Geophysical Research Letters*, 38, <https://doi.org/https://doi.org/10.1029/2011GL048794>, 2011.
- Cole, S. T., Wortham, C., Kunze, E., and Owens, W. B.: Eddy stirring and horizontal diffusivity from Argo float observations: Geographic and depth variability, *Geophysical Research Letters*, 42, 3989–3997, <https://doi.org/10.1002/2015GL063827>, 2015.
- 835 CORE2 Global Air-Sea Flux Dataset: CORE.2 Global Air-Sea Flux Dataset ds260.2 Published by the CISL Data Support Section at the National Center for Atmospheric Research, Boulder, CO, Accessed - 26 mar 2013, U.S. National Center for Atmospheric Research [Climate and Global Dynamics Division], U.S. Geophysical Fluid Dynamics Laboratory [NOMADS], U.K. Hadley Centre for Climate Prediction and Research, and U.S. National Centers for Environmental Prediction., <http://dss.ucar.edu/datasets/ds260.2/>.
- Dai, A.: Historical and Future Changes in Streamflow and Continental Runoff, pp. 17–37, John Wiley & Sons, Inc., ISBN 9781118971772,
840 <https://doi.org/10.1002/9781118971772.ch2>, 2016.

- Danabasoglu, G., Yeager, S. G., Bailey, D., Behrens, E., Bentsen, M., Bi, D., Biastoch, A., Böning, C., Bozec, A., Canuto, V. M., Cassou, C., Chassignet, E., Coward, A. C., Danilov, S., Diansky, N., Drange, H., Farneti, R., Fernandez, E., Fogli, P. G., Forget, G., Fujii, Y., Griffies, S. M., Gusev, A., Heimbach, P., Howard, A., Jung, T., Kelley, M., Large, W. G., Leboissetier, A., Lu, J., Madec, G., Marsland, S. J., Masina, S., Navarra, A., Nurser, A. G., Pirani, A., y Méliá, D. S., Samuels, B. L., Scheinert, M., Sidorenko, D., Treguier, A.-M., Tsujino, H., Uotila, P., Valcke, S., Voldoire, A., and Wang, Q.: North Atlantic simulations in Coordinated Ocean-ice Reference Experiments phase II (CORE-II). Part I: Mean states, *Ocean Modelling*, 73, 76 – 107, <https://doi.org/http://dx.doi.org/10.1016/j.ocemod.2013.10.005>, 2014.
- 845 de Boyer Montégut, C., Madec, G., Fischer, A. S., Lazar, A., and Iudicone, D.: Mixed layer depth over the global ocean: An examination of profile data and a profile-based climatology, *Journal of Geophysical Research: Oceans*, 109, n/a–n/a, <https://doi.org/10.1029/2004JC002378>, c12003, 2004.
- 850 de Lavergne, C., Madec, G., Le Sommer, J., Nurser, A. J. G., and Naveira Garabato, A. C.: On the consumption of Antarctic Bottom Water in the abyssal ocean, *Journal of Physical Oceanography*, <https://doi.org/10.1175/JPO-D-14-0201.1>, 2015.
- de Lavergne, C., Falahat, S., Madec, G., Roquet, F., Nycander, J., and Vic, C.: Toward global maps of internal tide energy sinks, *Ocean Modelling*, 137, 52–75, <https://doi.org/https://doi.org/10.1016/j.ocemod.2019.03.010>, 2019.
- de Lavergne, C., Vic, C., Madec, G., Roquet, F., Waterhouse, A. F., Whalen, C. B., Cuypers, Y., Bouruet-Aubertot, P., Ferron, B., and Hibiya, T.: A Parameterization of Local and Remote Tidal Mixing, *Journal of Advances in Modeling Earth Systems*, 12, e2020MS002065, <https://doi.org/10.1029/2020MS002065>, 2020.
- 855 de Lavergne, C., Groeskamp, S., Zika, J., and Johnson, H. L.: Chapter 3 - The role of mixing in the large-scale ocean circulation, in: *Ocean Mixing*, edited by Meredith, M. and Naveira Garabato, A., pp. 35–63, Elsevier, ISBN 978-0-12-821512-8, <https://doi.org/https://doi.org/10.1016/B978-0-12-821512-8.00010-4>, 2022.
- 860 Dewar, W. K., Hsueh, Y., McDougall, T. J., and Yuan, D.: Calculation of Pressure in Ocean Simulations, *Journal of Physical Oceanography*, 28, 577 – 588, [https://doi.org/10.1175/1520-0485\(1998\)028<0577:COPIOS>2.0.CO;2](https://doi.org/10.1175/1520-0485(1998)028<0577:COPIOS>2.0.CO;2), 1998.
- Domingues, C. M., Church, J. A., White, N. J., Gleckler, P. J., Wijffels, S. E., Barker, P. M., and Dunn, J. R.: Improved estimates of upper-ocean warming and multi-decadal sea-level rise, *Nature*, 453, 1090–, 2008.
- Eyring, V., Gillett, N., Achuta Rao, K., Barimalala, R., Barreiro Parrillo, M., Bellouin, N., Cassou, C., Durack, P., Kosaka, Y., McGregor, S., Min, S., Morgenstern, O., and Sun, Y.: Chapter 3: Human Influence on the Climate System, chap. Chapter 3: Human Influence on the Climate System, pp. 423–552, Cambridge University Press, ISBN 9781009157889, <https://doi.org/DOI:10.1017/9781009157896.005>, 2023.
- 865 Fasullo, J. T. and Nerem, R. S.: Altimeter-era emergence of the patterns of forced sea-level rise in climate models and implications for the future, *Proceedings of the National Academy of Sciences*, 115, 12944–12949, <https://doi.org/10.1073/pnas.1813233115>, 2018.
- 870 Ferrari, R. and Nikurashin, M.: Suppression of Eddy Diffusivity across Jets in the Southern Ocean, *Journal of Physical Oceanography*, 40, 1501–1519, <https://doi.org/10.1175/2010JPO4278.1>, 2010.
- Ferrari, R., McWilliams, J. C., Canuto, V. M., and Dubovikov, M.: Parameterization of Eddy Fluxes near Oceanic Boundaries, *Journal of Climate*, 21, 2770–2789, <https://doi.org/10.1175/2007JCLI1510.1>, 2008.
- Ferrari, R., Griffies, S. M., Nurser, A. G., and Vallis, G. K.: A boundary-value problem for the parameterized mesoscale eddy transport, *Ocean Modelling*, 32, 143 – 156, <https://doi.org/http://dx.doi.org/10.1016/j.ocemod.2010.01.004>, the magic of modelling: A special volume commemorating the contributions of Peter D. Killworth – Part 2, 2010.
- 875 Foster, T. D.: An Analysis of the Cabbeling Instability in Sea Water, *Journal of Physical Oceanography*, 2, 294–301, [https://doi.org/10.1175/1520-0485\(1972\)002<0294:AAOTCI>2.0.CO;2](https://doi.org/10.1175/1520-0485(1972)002<0294:AAOTCI>2.0.CO;2), 1972.

- 880 Fox-Kemper, B., Adcroft, A., Böning, C. W., Chassignet, E. P., Curchitser, E., Danabasoglu, G., Eden, C., England, M. H., Gerdes, R., Greatbatch, R. J., Griffies, S. M., Hallberg, R. W., Hanert, E., Heimbach, P., Hewitt, H. T., Hill, C. N., Komuro, Y., Legg, S., Le Sommer, J., Masina, S., Marsland, S. J., Penny, S. G., Qiao, F., Ringler, T. D., Treguier, A. M., Tsujino, H., Uotila, P., and Yeager, S. G.: Challenges and Prospects in Ocean Circulation Models, *Frontiers in Marine Science*, 6, 65, <https://doi.org/10.3389/fmars.2019.00065>, 2019.
- 885 Fox-Kemper, B., Hewitt, H., Xiao, C., Aðalgeirsdóttir, G., Drijfhout, S., Edwards, T., Golledge, N., Hemer, M., Kopp, R., Krinner, G., Mix, A., Notz, D., Nowicki, S., Nurhati, I., Ruiz, L., Sallée, J.-B., Slangen, A., and Yu, Y.: Chapter 9 - Ocean, Cryosphere and Sea Level Change, chap. Chapter 9 - Ocean, Cryosphere and Sea Level Change, pp. 1211–1362, Cambridge University Press, ISBN 9781009157889, [https://doi.org/DOI: 10.1017/9781009157896.011](https://doi.org/DOI:10.1017/9781009157896.011), 2023.
- Frederikse, T., Landerer, F., Caron, L., Adhikari, S., Parkes, D., Humphrey, V. W., Dangendorf, S., Hogarth, P., Zanna, L., Cheng, L., and Wu, Y.-H.: The causes of sea-level rise since 1900, *Nature*, 584, 393–397, <https://doi.org/10.1038/s41586-020-2591-3>, 2020.
- 890 Garcia, H., Boyer, T., Baranova, O., Locarnini, R., Mishonov, A., Grodsky, A., Paver, C., Weathers, K., Smolyar, I., Reagan, J., Seidov, D., and M.M., Z.: *World Ocean Atlas 2018: Product Documentation*, Tech. rep., A. Mishonov, Technical Editor, 2019.
- Gent, P. R. and McWilliams, J. C.: Isopycnal Mixing in Ocean Circulation Models., *Journal of Physical Oceanography*, 20, 150–155, [https://doi.org/10.1175/1520-0485\(1990\)020<0150:IMIOCM>2.0.CO;2](https://doi.org/10.1175/1520-0485(1990)020<0150:IMIOCM>2.0.CO;2), 1990.
- Gent, P. R., Willebrand, J., McDougall, T. J., and McWilliams, J. C.: Parameterizing Eddy-Induced Tracer Transports in Ocean Circulation Models., *Journal of Physical Oceanography*, 25, 463–474, [https://doi.org/10.1175/1520-0485\(1995\)025<0463:PEITTI>2.0.CO;2](https://doi.org/10.1175/1520-0485(1995)025<0463:PEITTI>2.0.CO;2), 1995.
- 895 Gill, A. E. and Niller, P. P.: The theory of the seasonal variability in the ocean, *Deep Sea Research and Oceanographic Abstracts*, 20, 141–177, [https://doi.org/https://doi.org/10.1016/0011-7471\(73\)90049-1](https://doi.org/https://doi.org/10.1016/0011-7471(73)90049-1), 1973.
- Gille, S. T.: How nonlinearities in the equation of state of seawater can confound estimates of steric sea level change, *Journal of Geophysical Research: Oceans*, 109, <https://doi.org/https://doi.org/10.1029/2003JC002012>, 2004.
- Goutorbe, B., Poort, J., Lucazeau, F., and Raillard, S.: Global heat flow trends resolved from multiple geological and geophysical proxies, *Geophysical Journal International*, 187, 1405–1419, <https://doi.org/10.1111/j.1365-246X.2011.05228.x>, 2011.
- 900 Graham, F. S. and McDougall, T. J.: Quantifying the Nonconservative Production of Conservative Temperature, Potential Temperature, and Entropy., *Journal of Physical Oceanography*, 43, 838–862, <https://doi.org/10.1175/JPO-D-11-0188.1>, 2013.
- Griffies, S. M.: The Gent–McWilliams Skew Flux., *Journal of Physical Oceanography*, 28, 831–841, [https://doi.org/10.1175/1520-0485\(1998\)028<0831:TGMSF>2.0.CO;2](https://doi.org/10.1175/1520-0485(1998)028<0831:TGMSF>2.0.CO;2), 1998.
- 905 Griffies, S. M.: *Fundamentals of ocean climate models.*, Princeton University Press, 2004.
- Griffies, S. M.: *Elements of the Modular Ocean Model (MOM)*, NOAA Geophysical Fluid Dynamics Laboratory, Princeton, USA, 2012.
- Griffies, S. M. and Greatbatch, R. J.: Physical processes that impact the evolution of global mean sea level in ocean climate models., *Ocean Modelling*, 51, 37–72, <https://doi.org/http://dx.doi.org/10.1016/j.ocemod.2012.04.003>, 2012.
- Groeskamp, S. and Iudicone, D.: The effect of air-sea flux products, short wave radiation depth penetration and albedo on the upper ocean overturning circulation, *Geophysical Research Letters*, 0, <https://doi.org/10.1029/2018GL078442>, 2018.
- 910 Groeskamp, S., Abernathy, R. P., and Klocker, A.: Water Mass Transformation by Cabbeling and Thermobaricity, *Geophysical Research Letters*, <https://doi.org/10.1002/2016GL070860>, 2016.
- Groeskamp, S., Sloyan, B. M., Zika, J. D., and McDougall, T. J.: Mixing Inferred from an Ocean Climatology and Surface Fluxes, *Journal of Physical Oceanography*, 47, 667–687, <https://doi.org/10.1175/JPO-D-16-0125.1>, 2017.
- 915 Groeskamp, S., Barker, P. M., McDougall, T. J., Abernathy, R. P., and Griffies, S. M.: VENM: An Algorithm to Accurately Calculate Neutral Slopes and Gradients, *Journal of Advances in Modeling Earth Systems*, 11, 1917–1939, <https://doi.org/10.1029/2019MS001613>, 2019a.

- Groeskamp, S., Griffies, S. M., Iudicone, D., Marsh, R., Nurser, A. J. G., and Zika, J. D.: The Water Mass Transformation Framework for Ocean Physics and Biogeochemistry, *Annual Review of Marine Science*, 11, 271–305, <https://doi.org/10.1146/annurev-marine-010318-095421>, 2019b.
- 920 Groeskamp, S., LaCasce, J. H., McDougall, T. J., and Rogé, M.: Full-Depth Global Estimates of Ocean Mesoscale Eddy Mixing From Observations and Theory, *Geophysical Research Letters*, 47, e2020GL089425, <https://doi.org/10.1029/2020GL089425>, 2020.
- Hamlington, B. D., Chambers, D. P., Frederikse, T., Dangendorf, S., Fournier, S., Buzzanga, B., and Nerem, R. S.: Observation-based trajectory of future sea level for the coastal United States tracks near high-end model projections, *Communications Earth & Environment*, 3, 230, <https://doi.org/10.1038/s43247-022-00537-z>, 2022.
- 925 Hamlington, B. D., Bellas-Manley, A., Willis, J. K., Fournier, S., Vinogradova, N., Nerem, R. S., Piecuch, C. G., Thompson, P. R., and Kopp, R.: The rate of global sea level rise doubled during the past three decades, *Communications Earth & Environment*, 5, 601, <https://doi.org/10.1038/s43247-024-01761-5>, 2024.
- Holmes, R. M., Groeskamp, S., Stewart, K. D., and McDougall, T. J.: Sensitivity of a Coarse-Resolution Global Ocean Model to a Spatially Variable Neutral Diffusivity, *Journal of Advances in Modeling Earth Systems*, 14, e2021MS002914, <https://doi.org/https://doi.org/10.1029/2021MS002914>, 2022.
- 930 Horwath, M., Gutknecht, B. D., Cazenave, A., Palanisamy, H. K., Marti, F., Marzeion, B., Paul, F., Le Bris, R., Hogg, A. E., Otosaka, I., Shepherd, A., Döll, P., Cáceres, D., Müller Schmied, H., Johannessen, J. A., Nilsen, J. E. Ø., Raj, R. P., Forsberg, R., Sandberg Sørensen, L., Barletta, V. R., Simonsen, S. B., Knudsen, P., Andersen, O. B., Randal, H., Rose, S. K., Merchant, C. J., Macintosh, C. R., von Schuckmann, K., Novotny, K., Groh, A., Restano, M., and Benveniste, J.: Global sea-level budget and ocean-mass budget, with a focus on advanced data products and uncertainty characterisation, *Earth System Science Data*, 14, 411–447, <https://doi.org/10.5194/essd-14-411-2022>, 2022.
- 935 Hu, C., Lee, Z., and Franz, B.: Chlorophyll-a algorithms for oligotrophic oceans: A novel approach based on three-band reflectance difference, *Journal of Geophysical Research: Oceans*, 117, n/a–n/a, <https://doi.org/10.1029/2011JC007395>, 2012.
- Huang, R. X.: Real Freshwater Flux as a Natural Boundary Condition for the Salinity Balance and Thermohaline Circulation Forced by Evaporation and Precipitation., *Journal of Physical Oceanography*, 23, 2428–2446, [https://doi.org/10.1175/1520-0485\(1993\)023<2428:RFFAAN>2.0.CO;2](https://doi.org/10.1175/1520-0485(1993)023<2428:RFFAAN>2.0.CO;2), 1993.
- IOC, SCOR, and IAPSO: The international thermodynamic equation of seawater – 2010: Calculation and use of thermodynamic properties., Intergovernmental Oceanographic Commission, Manuals and Guides. UNESCO (English), [Available online at www.TEOS-10.org], 2010.
- 945 Ishii, M. and Kimoto, M.: Reevaluation of historical ocean heat content variations with time-varying XBT and MBT depth bias corrections, *Journal of Oceanography*, 65, 287–299, <https://doi.org/10.1007/s10872-009-0027-7>, 2009.
- Iudicone, D., Rodgers, K. B., Stendardo, I., Aumont, O., Madec, G., Bopp, L., Mangoni, O., and Ribera d’Alcala’, M.: Water masses as a unifying framework for understanding the Southern Ocean Carbon Cycle, *Biogeosciences*, 8, 1031–1052, <https://doi.org/10.5194/bg-8-1031-2011>, 2011.
- 950 Jackett, D. R. and McDougall, T. J.: Minimal Adjustment of Hydrographic Profiles to Achieve Static Stability., *Journal of Atmospheric and Oceanic Technology*, 12, 381–389, [https://doi.org/10.1175/1520-0426\(1995\)012<0381:MAOHPT>2.0.CO;2](https://doi.org/10.1175/1520-0426(1995)012<0381:MAOHPT>2.0.CO;2), 1995.
- Jayne, S. R., St. Laurent, L. C. and, F., and Gille, S. T.: Connections Between Ocean Bottom Topography and Earth’s Climate, *Oceanography*, issue volume, 2004.
- Jerlov, N. G.: *Optical oceanography*, American Elsevier Publ. Co., Inc., New York., 1968.

- 955 Jevrejeva, S., Grinsted, A., Moore, J. C., and Holgate, S.: Nonlinear trends and multiyear cycles in sea level records, *Journal of Geophysical Research: Oceans*, 111, <https://doi.org/https://doi.org/10.1029/2005JC003229>, 2006.
- Josey, S. A., Kent, E. C., and Taylor, P. K.: New Insights into the Ocean Heat Budget Closure Problem from Analysis of the SOC Air–Sea Flux Climatology, *Journal of Climate*, 12, 2856 – 2880, [https://doi.org/10.1175/1520-0442\(1999\)012<2856:NIITOH>2.0.CO;2](https://doi.org/10.1175/1520-0442(1999)012<2856:NIITOH>2.0.CO;2), 1999.
- Klocker, A. and Abernathy, R.: Global Patterns of Mesoscale Eddy Properties and Diffusivities., *Journal of Physical Oceanography*, 44, 960 1030–1046, <https://doi.org/10.1175/JPO-D-13-0159.1>, 2013.
- Klocker, A. and McDougall, T. J.: Influence of the Nonlinear Equation of State on Global Estimates of Dianeutral Advection and Diffusion, *Journal of Physical Oceanography*, 40, 1690–1709, <https://doi.org/10.1175/2010JPO4303.1>, 2010.
- Klocker, A., McDougall, T. J., and Jackett, D. R.: A new method for forming approximately neutral surfaces, *Ocean Science*, 5, 155–172, <https://doi.org/10.5194/os-5-155-2009>, 2009.
- 965 Klocker, A., Ferrari, R., and LaCasce, J. H.: Estimating Suppression of Eddy Mixing by Mean Flows, *Journal of Physical Oceanography*, 42, 1566–1576, <https://doi.org/10.1175/JPO-D-11-0205.1>, 2012.
- Kusters, N., Groeskamp, S., and McDougall, T. J.: Spiralling Inverse Method: A New Inverse Method to Estimate Ocean Mixing, *Journal of Physical Oceanography*, 54, 2289–2309, <https://doi.org/https://doi.org/10.1175/JPO-D-24-0009.1>, 2024.
- Kusters, N., Balwada, D., and Groeskamp, S.: Global Observational Estimates of Mesoscale Eddy-Driven Quasi-Stokes Velocity and Buoy-
970 ancy Diffusivity, *Geophysical Research Letters*, 52, e2025GL115 802, <https://doi.org/https://doi.org/10.1029/2025GL115802>, 2025.
- LaCasce, J. H. and Groeskamp, S.: Baroclinic modes over rough bathymetry and the surface deformation radius, *Journal of Physical Oceanography*, pp. 1–40, <https://doi.org/10.1175/JPO-D-20-0055.1>, 2020.
- Large, W., McWilliams, J., and Doney, S.: Oceanic vertical mixing: a review and a model with a nonlocal boundary layer parameterization, *Reviews of Geophysics*, 32, 363–403, 1994.
- 975 Large, W. G. and Yeager, S.: The global climatology of an interannually varying air-sea flux data set, *Climate Dynamics*, 33, 341–364, <https://doi.org/10.1007/s00382-008-0441-3>, 2009.
- Large, W. G. and Yeager, S. G.: Diurnal to decadal global forcing for ocean and sea-ice models: the data sets and flux climatologies, 2004.
- Lebedev, K. V., Yoshinari, H., Maximenko, N. A., and Hacker, P. W.: YoMaHa’07: Velocity data assessed from trajectories of Argo floats at parking level and at the sea, *IPRC Tech. Note 4(2)*, <http://apdrc.soest.hawaii.edu/projects/yomaha/yomaha07/YoMaHa070612small.pdf>,
980 16, 2007.
- Levitus, S., Antonov, J. I., Boyer, T. P., Baranova, O. K., Garcia, H. E., Locarnini, R. A., Mishonov, A. V., Reagan, J. R., Seidov, D., Yarosh, E. S., and Zweng, M. M.: World ocean heat content and thermosteric sea level change (0–2000 m), 1955–2010, *Geophysical Research Letters*, 39, n/a–n/a, <https://doi.org/10.1029/2012GL051106>, 2012.
- Lévy, M., Resplandy, L., Palter, J. B., Couespel, D., and Lachkar, Z.: Chapter 13 - The crucial contribution of mixing to present and future
985 ocean oxygen distribution, pp. 329–344, Elsevier, ISBN 978-0-12-821512-8, <https://doi.org/https://doi.org/10.1016/B978-0-12-821512-8.00020-7>, 2022.
- Lewis, M. R., Carr, M.-E., Feldman, G. C., Esaias, W., and McClain, C.: Influence of penetrating solar radiation on the heat budget of the equatorial Pacific Ocean, *Nature*, 347, 543–545, 1990.
- Li, Z., England, M. H., and Groeskamp, S.: Recent acceleration in global ocean heat accumulation by mode and intermediate waters, *Nature
990 Communications*, 14, 6888, <https://doi.org/10.1038/s41467-023-42468-z>, 2023.
- Ludwigsen, C. B., Andersen, O. B., Marzeion, B., Malles, J.-H., Müller Schmied, H., Döll, P., Watson, C., and King, M. A.: Global and regional ocean mass budget closure since 2003, *Nature Communications*, 15, 1416, <https://doi.org/10.1038/s41467-024-45726-w>, 2024.

- Lyman, J. M. and Johnson, G. C.: Estimating Global Ocean Heat Content Changes in the Upper 1800 m since 1950 and the Influence of Climatology Choice, *Journal of Climate*, 27, 1945–1957, <https://doi.org/10.1175/JCLI-D-12-00752.1>, 2013.
- 995 MacKinnon, J., Laurent, L. S., and Garabato, A. N.: Diapycnal mixing processes in the ocean interior., in: *Ocean Circulation and Climate: A 21st Century Perspective*. 2nd Ed, edited by Siedler, G., Griffies, S., Gould, J., and Church, J., pp. 159–184, Academic Press, 2nd ed. edn., 2013.
- McDougall, T. and Barker, P. M.: *Getting started with TEOS-10 and the Gibbs Seawater (GSW) Oceanographic Toolbox.*, SCOR/IAPSO, WG127, ISBN 978-0-646-55621-5, 2011.
- 1000 McDougall, T. J.: The Relative Roles of Diapycnal and Isopycnal Mixing on Subsurface Water Mass Conversion., *Journal of Physical Oceanography*, 14, 1577–1589, [https://doi.org/10.1175/1520-0485\(1984\)014<1577:TRRODA>2.0.CO;2](https://doi.org/10.1175/1520-0485(1984)014<1577:TRRODA>2.0.CO;2), 1984.
- McDougall, T. J.: Neutral Surfaces., *Journal of Physical Oceanography*, 17, 1950–1964, [https://doi.org/10.1175/1520-0485\(1987\)017<1950:NS>2.0.CO;2](https://doi.org/10.1175/1520-0485(1987)017<1950:NS>2.0.CO;2), 1987a.
- McDougall, T. J.: Thermobaricity, cabbeling, and water-mass conversion., *Journal of Geophysical Research: Oceans*, 92, 5448–5464, <https://doi.org/10.1029/JC092iC05p05448>, 1987b.
- 1005 McDougall, T. J.: Potential Enthalpy: A Conservative Oceanic Variable for Evaluating Heat Content and Heat Fluxes., *Journal of Physical Oceanography*, 33, 945–963, [https://doi.org/10.1175/1520-0485\(2003\)033<0945:PEACOV>2.0.CO;2](https://doi.org/10.1175/1520-0485(2003)033<0945:PEACOV>2.0.CO;2), 2003.
- McDougall, T. J. and Garrett, C. J.: Scalar conservation equations in a turbulent ocean, *Deep Sea Research Part A. Oceanographic Research Papers*, 39, 1953 – 1966, [https://doi.org/http://dx.doi.org/10.1016/0198-0149\(92\)90007-G](https://doi.org/http://dx.doi.org/10.1016/0198-0149(92)90007-G), 1992.
- 1010 McDougall, T. J. and Jackett, D. R.: On the helical nature of neutral trajectories in the ocean., *Progress In Oceanography*, 20, 153 – 183, [https://doi.org/DOI: 10.1016/0079-6611\(88\)90001-8](https://doi.org/DOI:10.1016/0079-6611(88)90001-8), 1988.
- McDougall, T. J. and McIntosh, P. C.: The Temporal-Residual-Mean Velocity. Part II: Isopycnal Interpretation and the Tracer and Momentum Equations., *Journal of Physical Oceanography*, 31, 1222–1246, [https://doi.org/10.1175/1520-0485\(2001\)031<1222:TTRMVP>2.0.CO;2](https://doi.org/10.1175/1520-0485(2001)031<1222:TTRMVP>2.0.CO;2), 2001.
- 1015 McDougall, T. J., Jackett, D. R., Millero, F. J., Pawlowicz, R., and Barker, P. M.: A global algorithm for estimating Absolute Salinity., *Ocean Science*, 8, 1117–1128, 2012.
- McDougall, T. J., Groeskamp, S., and Griffies, S. M.: On Geometrical Aspects of Interior Ocean Mixing, *Journal of Physical Oceanography*, 44, 2164–2175, <https://doi.org/10.1175/JPO-D-13-0270.1>, 2014.
- Melet, A. V., Hallberg, R., and Marshall, D. P.: Chapter 2 - The role of ocean mixing in the climate system, pp. 5–34, Elsevier, ISBN 978-0-12-821512-8, <https://doi.org/https://doi.org/10.1016/B978-0-12-821512-8.00009-8>, 2022.
- 1020 Millero, F. J., Feistel, R., Wright, D. G., and McDougall, T. J.: The composition of Standard Seawater and the definition of the Reference-Composition Salinity Scale, *Deep Sea Research Part I: Oceanographic Research Papers*, 55, 50–72, 2008.
- Moore, J. C., Jevrejeva, S., and Grinsted, A.: The historical global sea-level budget, *Annals of Glaciology*, 52, 8–14, [https://doi.org/DOI: 10.3189/172756411799096196](https://doi.org/DOI:10.3189/172756411799096196), 2011.
- 1025 Morel, A. and Antoine, D.: Heating Rate within the Upper Ocean in Relation to its Bio–optical State, *Journal of Physical Oceanography*, 24, 1652–1665, [https://doi.org/10.1175/1520-0485\(1994\)024<1652:HRWTUO>2.0.CO;2](https://doi.org/10.1175/1520-0485(1994)024<1652:HRWTUO>2.0.CO;2), 1994.
- Nerem, R. S., Beckley, B. D., Fasullo, J. T., Hamlington, B. D., Masters, D., and Mitchum, G. T.: Climate-change–driven accelerated sea-level rise detected in the altimeter era, *Proceedings of the National Academy of Sciences*, 115, 2022–2025, <https://doi.org/10.1073/pnas.1717312115>, 2018.

- 1030 Nerem, R. S., Frederikse, T., and Hamlington, B. D.: Extrapolating Empirical Models of Satellite-Observed Global Mean Sea Level to Estimate Future Sea Level Change, *Earth's Future*, 10, e2021EF002 290, <https://doi.org/https://doi.org/10.1029/2021EF002290>, 2022.
- Nurser, A. J. G. and Griffies, S. M.: Relating the diffusive salt flux just below the ocean surface to boundary freshwater and salt fluxes, *Journal of Physical Oceanography*, <https://doi.org/10.1175/JPO-D-19-0037.1>, 2019.
- Ohlmann, J. C.: Ocean Radiant Heating in Climate Models, *Journal of Climate*, 16, 1337–1351, <https://doi.org/10.1175/1520-0442-1035> 16.9.1337, 2003.
- Pattullo, J., Munk, W., Revelle, R., and Strong, E.: The seasonal oscillation in sea level., *Journal of Marine Research*, 14, 1955.
- Paulson, C. A. and Simpson, J. J.: Irradiance Measurements in the Upper Ocean, *Journal of Physical Oceanography*, 7, 952–956, [https://doi.org/10.1175/1520-0485\(1977\)007<0952:IMITUO>2.0.CO;2](https://doi.org/10.1175/1520-0485(1977)007<0952:IMITUO>2.0.CO;2), 1977.
- Polzin, K. L., Toole, J. M., Ledwell, J. R., and Schmitt, R. W.: Spatial Variability of Turbulent Mixing in the Abyssal Ocean., *Science*, 276, 93–96, <http://www.sciencemag.org/content/276/5309/93.abstract>, 1997.
- 1040 Pradal, M.-A. and Gnanadesikan, A.: How does the Redi parameter for mesoscale mixing impact global climate in an Earth System Model?, *Journal of Advances in Modeling Earth Systems*, 6, 586–601, <https://doi.org/10.1002/2013MS000273>, 2014.
- Prandtl, L.: Report on investigation of developed turbulence, *Mechanik*, 5, 1925.
- Redi, M. H.: Oceanic Isopycnal Mixing by Coordinate Rotation., *Journal of Physical Oceanography*, 12, 1154–1158, [https://doi.org/10.1175/1520-0485\(1982\)012<1154:OIMBCR>2.0.CO;2](https://doi.org/10.1175/1520-0485(1982)012<1154:OIMBCR>2.0.CO;2), 1982.
- 1045 Roach, C. J., Balwada, D., and Speer, K.: Global Observations of Horizontal Mixing from Argo Float and Surface Drifter Trajectories, *Journal of Geophysical Research: Oceans*, 123, 4560–4575, <https://doi.org/10.1029/2018JC013750>, 2018.
- Schanze, J. J. and Schmitt, R. W.: Estimates of Cabbeling in the Global Ocean, *Journal of Physical Oceanography*, 43, 698–705, <https://doi.org/10.1175/JPO-D-12-0119.1>, 2013.
- 1050 Services, C. M.: E.U. Copernicus Marine Service Information (CMEMS)., Tech. rep., Marine Data Store (MDS)., <https://doi.org/10.48670/moi-00148> (Accessed on 09-Dec-2024).
- Sévellec, F., Verdière, A. C. d., and Kolodziejczyk, N.: Estimation of Horizontal Turbulent Diffusivity from Deep Argo Float Displacements, *Journal of Physical Oceanography*, 52, 1509–1529, <https://doi.org/https://doi.org/10.1175/JPO-D-21-0150.1>, 2022.
- Shao, A. E., Adcroft, A., Hallberg, R., and Griffies, S. M.: A General-Coordinate, Nonlocal Neutral Diffusion Operator, *Journal of Advances in Modeling Earth Systems*, 12, e2019MS001 992, <https://doi.org/https://doi.org/10.1029/2019MS001992>, 2020.
- 1055 Shepherd, A., Ivins, E., Rignot, E., Smith, B., van den Broeke, M., Velicogna, I., Whitehouse, P., Briggs, K., Joughin, I., Krinner, G., Nowicki, S., Payne, T., Scambos, T., Schlegel, N., A. G., Agosta, C., Ahlstrøm, A., Babonis, G., Barletta, V., Blazquez, A., Bonin, J., Csatho, B., Cullather, R., Felikson, D., Fettweis, X., Forsberg, R., Gallee, H., Gardner, A., Gilbert, L., Groh, A., Gunter, B., Hanna, E., Harig, C., Helm, V., Horvath, A., Horwath, M., Khan, S., Kjeldsen, K. K., Konrad, H., Langen, P., Lecavalier, B., Loomis, B., Luthcke, S., McMillan, M., Melini, D., Mernild, S., Mohajerani, Y., Moore, P., Mougnot, J., Moyano, G., Muir, A., Nagler, T., Nield, G., Nilsson, J., Noel, B., Otosaka, I., Pattle, M. E., Peltier, W. R., Pie, N., Rietbroek, R., Rott, H., Sandberg-Sørensen, L., Sasgen, I., Save, H., Scheuchl, B., Schrama, E., Schröder, L., Seo, K.-W., Simonsen, S., Slater, T., Spada, G., Sutterley, T., Talpe, M., Tarasov, L., van de Berg, W. J., van der Wal, W., van Wesse, M., Vishwakarma, B. D., Wiese, D., Wouters, B., and team, T. I.: Mass balance of the Antarctic Ice Sheet from 1992 to 2017, *Nature*, 558, 219–222, <https://doi.org/10.1038/s41586-018-0179-y>, 2018.
- 1060 Smith, K. S. and Marshall, J.: Evidence for Enhanced Eddy Mixing at Middepth in the Southern Ocean, *Journal of Physical Oceanography*, 39, 50–69, <https://doi.org/10.1175/2008JPO3880.1>, 2009.

- Spingys, C. P., Williams, R. G., Tuerena, R. E., Naveira Garabato, A., Vic, C., Forryan, A., and Sharples, J.: Observations of Nutrient Supply by Mesoscale Eddy Stirring and Small-Scale Turbulence in the Oligotrophic North Atlantic, *Global Biogeochemical Cycles*, 35, e2021GB007200, <https://doi.org/https://doi.org/10.1029/2021GB007200>, 2021.
- 1070 Stanley, G. J.: Neutral surface topology, *Ocean Modelling*, 138, 88–106, <https://doi.org/https://doi.org/10.1016/j.ocemod.2019.01.008>, 2019.
- Stanley, Z., Bachman, S. D., and Grooms, I.: Vertical Structure of Ocean Mesoscale Eddies with Implications for Parameterizations of Tracer Transport, *Journal of Advances in Modeling Earth Systems*, 12, e2020MS002151, <https://doi.org/10.1029/2020MS002151>, 2020.
- Sweeney, C., Gnanadesikan, A., Griffies, S. M., Harrison, M. J., Rosati, A. J., and Samuels, B. L.: Impacts of Shortwave Penetration Depth on Large-Scale Ocean Circulation and Heat Transport, *Journal of Physical Oceanography*, 35, 1103–1119, <https://doi.org/10.1175/JPO2740.1>, 2005.
- 1075 Tandon, A. and Garrett, C.: Water mass formation from thermodynamics: a framework for examining compatibility with dynamics, *WOCE*, p. 34, 1997.
- Tang, R., Wang, Y., Jiang, Y., Liu, M., Peng, Z., Hu, Y., Huang, L., and Li, Z.-L.: A review of global products of air-sea turbulent heat flux: accuracy, mean, variability, and trend, *Earth-Science Reviews*, 249, 104662, <https://doi.org/https://doi.org/10.1016/j.earscirev.2023.104662>, 2024.
- 1080 Treguier, A. M., Held, I., and Larichev, V.: Parameterization of Quasigeostrophic Eddies in Primitive Equation Ocean Models, *J. Phys. Oceanogr.*, 27, 567–580, 1997.
- Urakawa, L. S. and Hasumi, H.: Eddy-Resolving Model Estimate of the Cabbeling Effect on the Water Mass Transformation in the Southern Ocean, *Journal of Physical Oceanography*, 42, 1288–1302, <https://doi.org/10.1175/JPO-D-11-0173.1>, 2012.
- 1085 Valdivieso, M., Haines, K., Balmaseda, M., Chang, Y.-S., Drevillon, M., Ferry, N., Fujii, Y., Köhl, A., Storto, A., Toyoda, T., Wang, X., Waters, J., Xue, Y., Yin, Y., Barnier, B., Hernandez, F., Kumar, A., Lee, T., Masina, S., and Andrew Peterson, K.: An assessment of air–sea heat fluxes from ocean and coupled reanalyses, *Climate Dynamics*, 49, 983–1008, <https://doi.org/10.1007/s00382-015-2843-3>, 2017.
- Van Roekel, L., Adcroft, A. J., Danabasoglu, G., Griffies, S. M., Kauffman, B., Large, W., Levy, M., Reichl, B. G., Ringler, T., and Schmidt, M.: The KPP Boundary Layer Scheme for the Ocean: Revisiting Its Formulation and Benchmarking One-Dimensional Simulations Relative to LES, *Journal of Advances in Modeling Earth Systems*, 10, 2647–2685, <https://doi.org/https://doi.org/10.1029/2018MS001336>, 2018.
- 1090 von Schuckmann, K., Cheng, L., Palmer, M. D., Hansen, J., Tassone, C., Aich, V., Adusumilli, S., Beltrami, H., Boyer, T., Cuesta-Valero, F. J., Desbruyères, D., Domingues, C., García-García, A., Gentine, P., Gilson, J., Gorfer, M., Haimberger, L., Ishii, M., Johnson, G. C., Killick, R., King, B. A., Kirchengast, G., Kolodziejczyk, N., Lyman, J., Marzeion, B., Mayer, M., Monier, M., Monselesan, D. P., Purkey, S., 1095 Roemmich, D., Schweiger, A., Seneviratne, S. I., Shepherd, A., Slater, D. A., Steiner, A. K., Straneo, F., Timmermans, M.-L., and Wijffels, S. E.: Heat stored in the Earth system: where does the energy go?, *Earth System Science Data*, 12, 2013–2041, <https://doi.org/10.5194/essd-12-2013-2020>, 2020.
- Whalen, C. B., Talley, L. D., and MacKinnon, J. A.: Spatial and temporal variability of global ocean mixing inferred from Argo profiles, *Geophysical Research Letters*, 39, n/a–n/a, <https://doi.org/10.1029/2012GL053196>, 2012.
- 1100 Witte, E.: *Zur Theorie den Stromkabelungen*, Gaea: Natur und Leben., 1902.
- Yeager, S. G. and Large, W. G.: CORE.2 Global Air-Sea Flux Dataset., Dataset. <http://dx.doi.org/10.5065/D6WH2N0S>. Dataset. <http://dx.doi.org/10.5065/D6WH2N0S>. Accessed - 26 Mar 2013, Research Data Archive at the National Center for Atmospheric Research, Computational and Information Systems Laboratory., 2008.

- 1105 Yu, L.: Global Air–Sea Fluxes of Heat, Fresh Water, and Momentum: Energy Budget Closure and Unanswered Questions, *Annual Review of Marine Science*, 11, 227–248, <https://doi.org/https://doi.org/10.1146/annurev-marine-010816-060704>, 2019.
- Yu, L. and Weller, R. A.: Objectively Analyzed Air-Sea Heat Fluxes for the Global Ice-Free Oceans (1981-2005), *Bull. Amer. Meteor. Soc.*, 88, 527–539, 2007.
- 1110 Yu, L., Jin, X., and Weller, R. A.: Multidecade global flux datasets from the Objectively Analyzed Air-sea Fluxes (OAFlux) project: Latent and sensible heat fluxes, ocean evaporation, and related surface meteorological variables, Woods Hole Oceanographic Institution, Massachusetts, oa-2008-01 edn., 2008.
- Zhang, Y., Rossow, W. B., Lacis, A. A., Oinas, V., and Mishchenko, M. I.: Calculation of radiative fluxes from the surface to top of atmosphere based on ISCCP and other global data sets: Refinements of the radiative transfer model and the input data, *Journal of Geophysical Research: Atmospheres*, 109, n/a–n/a, <https://doi.org/10.1029/2003JD004457>, d19105, 2004.
- 1115 Zhang, Y., Rossow, W. B., and Stackhouse, P. W.: Comparison of different global information sources used in surface radiative flux calculation: Radiative properties of the surface, *Journal of Geophysical Research: Atmospheres*, 112, n/a–n/a, <https://doi.org/10.1029/2005JD007008>, d01102, 2007.
- Zhang, Y.-C., Rossow, W. B., and Lacis, A. A.: Calculation of surface and top of atmosphere radiative fluxes from physical quantities based on ISCCP data sets: 1. Method and sensitivity to input data uncertainties, *Journal of Geophysical Research: Atmospheres*, 100, 1149–1165, <https://doi.org/10.1029/94JD02747>, 1995.